catalysts

MDPI

Review

Progress in Developing $LnBaCo_2O_{5+\delta}$ as an Oxygen Reduction Catalyst for Solid Oxide Fuel Cells

Fa Zheng [1,2] and Shengli Pang [2,*]

[1] R&D Department, Jiangsu Yushi Energy Group Co., Ltd., Nantong 226500, China
[2] Institute for Advanced Materials, School of Materials Science and Engineering, Jiangsu University, Zhenjiang 212013, China
* Correspondence: slpang@ujs.edu.cn

Abstract: Solid oxide fuel cells (SOFCs) represent a breed of eco-friendly, weather-independent, decentralized power generation technologies, distinguished for their broad fuel versatility and superior electricity generation efficiency. At present, SOFCs are impeded by a lack of highly efficient oxygen reduction catalysts, a factor that significantly constrains their performance. The double perovskites $LnBaCo_2O_{5+\delta}$ (Ln = Lanthanide), renowned for their accelerated oxygen exchange and conductivity features, are widely acclaimed as a promising category of cathode catalysts for SOFCs. This manuscript offers a novel perspective on the physicochemical attributes of $LnBaCo_2O_{5+\delta}$ accumulated over the past two decades and delineates the latest advancements in fine-tuning the composition and nanostructure for SOFC applications. It highlights surface chemistry under operational conditions and microstructure as emerging research focal points towards achieving high-performance $LnBaCo_2O_{5+\delta}$ catalysts. This review offers a comprehensive insight into the latest advancements in utilizing $LnBaCo_2O_{5+\delta}$ in the field of SOFCs, presenting a clear roadmap for future developmental trajectories. Furthermore, it provides valuable insights for the application of double perovskite materials in domains such as water electrolysis, CO_2 electrolysis, chemical sensors, and metal–air batteries.

Keywords: solid oxide fuel cells; double perovskite; oxygen reduction reaction; electrocatalyst

check for updates

Citation: Zheng, F.; Pang, S. Progress in Developing $LnBaCo_2O_{5+\delta}$ as an Oxygen Reduction Catalyst for Solid Oxide Fuel Cells. *Catalysts* **2023**, *13*, 1288. https://doi.org/10.3390/catal13091288

Academic Editor: Chao Su

Received: 9 August 2023
Revised: 31 August 2023
Accepted: 5 September 2023
Published: 9 September 2023

1. Introduction

The escalating issues of climate change and energy shortages, predominantly driven by the pervasive and inefficient use of fossil fuels, have intensified the search for novel energy conversion methodologies. Among various power generation technologies, solid oxide fuel cells (SOFCs) hold a unique position. They are particularly noted for their exceptional efficiency rates: 45% to 65% for independent applications and exceeding 85% for combined heat and power applications. Moreover, their fuel compatibility is versatile, ranging from hydrogen to hydrocarbons and even to carbon, making SOFCs a pivotal component in the design of innovative energy solutions [1–3]. An SOFC is a solid-state device comprising two porous electrodes and a dense electrolyte. This electrolyte conducts solid oxygen ions and is the key functional component of each individual cell. Oxygen introduced at the cathode side is reduced to form O^{2-}. Driven by the concentration gradient, these O^{2-} ions travel through the dense electrolyte layer to reach the anode. At the anode side, the fuel is directly oxidized to H_2O and/or CO_2 by O^{2-}, releasing electrons to the external circuit [1,2]. Traditional SOFCs typically use the following materials: oxygen ion conductor yttria-stabilized zirconia (YSZ) for the electrolyte, the pure electronic conductors strontium-substituted manganites (LSM) for the cathode, and NiO–YSZ for the anode. Due to the inherent properties of these components, high operating temperatures, approximately 1000 °C, are required to achieve an economically viable power density [4]. However, such high operating temperatures result in significant fabrication and operational costs, severe material complications, and extended start–stop durations, all of which hinder the widespread commercialization of SOFCs [1,4,5].

In recent years, significant efforts have been made to lower the operational temperature of SOFCs to a range of 500–800 °C [1,4,6]. Identifying innovative oxygen catalysts with high catalytic activity at these reduced temperatures is a critical challenge for SOFCs, particularly due to the exceptionally high activation energy of LSM [1,2,5,7]. For instance, as the operational temperature decreases from 1000 °C to 500 °C, the polarization resistance of LSM increases dramatically from 1 Ω cm^2 to 2000 Ω cm^2. This decline in cathode catalytic performance is largely attributed to the limitation of the oxygen reduction reaction (ORR) to the narrow triple-phase boundary (TPB) at the interface between the cathode, electrolyte, and oxygen gas (air). Within this TPB, the transportation of electrons, oxygen vacancies or ions, and oxygen gas occurs, facilitating their movement to or from the reaction site [5,8].

Mixed ionic and electronic conductors (MIECs) that exhibit elevated oxygen ion conductivity within the temperature range of 500–800 °C have the potential to expand the oxygen reduction region from the TPB to several micrometers within the cathode. Consequently, these materials are anticipated to display exceptional catalytic activity for the ORR [9–13]. For instance, at a temperature of 700 °C, the area-specific resistance (ASR) of a $La_{0.6}Sr_{0.4}Co_{0.2}Fe_{0.8}O_{3-\delta}$ cathode on a gadolinium-doped ceria (GDC) electrolyte has been reported to be approximately 0.1 Ω cm^2 [12]. Furthermore, Pang et al. reported a notably lower resistance of less than 0.035 Ω cm^2 for $La_{0.5}Ba_{0.5}CoO_{3-\delta}$ on a GDC electrolyte under identical operating conditions [13]. In the search for advanced cathode materials for SOFCs, significant advancements have been realized over the past decade. However, polarization resistances at lower temperature ranges are often considered suboptimal. Notably, Hwang et al. observed a significant rise in the ASR of a $La_{0.6}Sr_{0.4}Coe_{0.2}Fe_{0.8}O_{3-\delta}$ cathode on a GDC electrolyte, increasing from ~0.1 Ω cm^2 at 700 °C to 12 Ω cm^2 at 500 °C [12]. The primary reason for this observation originates in the pronounced decrease in O^{2-} conductivity as the temperature drops, due to the relatively high activation energies associated with oxygen transport and exchange processes [12,14]. As such, the ongoing quest for high-performance cathodes for SOFCs underscores the need for the development of materials that facilitate faster oxygen transport and surface exchange.

Over the past few years, owing to its unique crystal structure, considerable efforts have been directed towards investigating the MIEC double perovskite oxides $LnBaCo_2O_{5+\delta}$ (Ln = Lanthanide). These materials find potential applications across a multitude of domains, such as magnetism [15–17], SOFCs, proton-conductive ceramic fuel cells [18–25], water electrolysis [26–28], CO_2 electrolysis [29], chemical sensors [30–32], ceramic semi-permeable membranes [33–35], metal–air batteries [36,37], soot combustion [38], supercapacitors [39], photocatalysis [40], and solar-driven thermal storage [41,42]. Given the diverse requirements in terms of physicochemical properties for each application, this article will exclusively focus on novel strategies employed in advancing double perovskites for use as cathode catalysts in SOFCs. It is worth noting that, due to the considerable interest in double perovskites, comprehensive reviews of these materials have previously been published [43,44]. However, the ongoing advancements in understanding the properties and applications of these materials underscore the need for updated reviews, such as the one presented in this article. Our discussions will span the exploration of physicochemical properties, optimization of composition, and enhancement of application methodologies. Additionally, we will deliberate on potential research breakthroughs concerning high-performance double perovskite-based cathode materials.

2. Physicochemical Properties of $LnBaCo_2O_{5+\delta}$

As depicted in Figure 1, the $LnBaCo_2O_{5+\delta}$ compound exhibits a perovskite structure of the 112 type. Relative to their disordered analogs, these orderly structures have been widely reported to considerably enhance the rate of oxygen transport [45,46]. Notably, Taskin et al. [45] were pioneers in observing a notably high oxygen diffusion coefficient (D_{chem}) of approximately 3.0×10^{-9} cm^2 s^{-1} at 350 °C and 10^{-5} cm^2 s^{-1} at 600 °C for the $GdBaCo_2O_{5+\delta}$ double perovskite. The oxygen transport characteristics of the $PrBaCo_2O_{5+\delta}$ double perovskite were subsequently evaluated by Kim et al. [47,48]. Their results demon-

strated appreciably higher rates of oxygen transport (D_{chem}) for $PrBaCo_2O_{5+\delta}$ in comparison to $GdBaCo_2O_{5+\delta}$, suggesting an enhancement in oxygen transport properties corresponding to the increased size of the Ln cation. Tarancón et al. carried out a detailed comparative study between the double perovskite $LnBaCo_2O_{5+\delta}$ (Ln = Pr, Gd) and other classes of oxygen catalysts [44]. As illustrated in Figure 2, the double perovskite outperformed in terms of oxygen transport properties, emphasizing its considerable potential as a cutting-edge cathode material for SOFCs. It is important to recognize that significant variations exist in the $LnBaCo_2O_{5+\delta}$ oxygen tracer diffusion and the oxygen surface exchange coefficient as reported by different research groups [49]. Such disparities mainly stem from differences in the precise composition and/or microstructure of the samples used by distinct researchers. Thus, readers are encouraged to assess the data in Figure 2 judiciously and objectively.

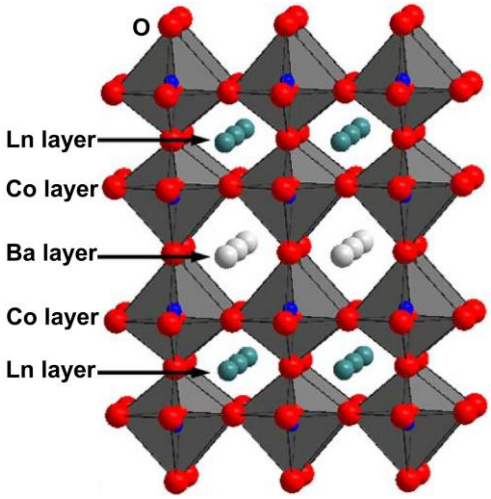

Figure 1. Schematic diagram of crystal structure for double perovskite oxide $LnBaCo_2O_{5+\delta}$.

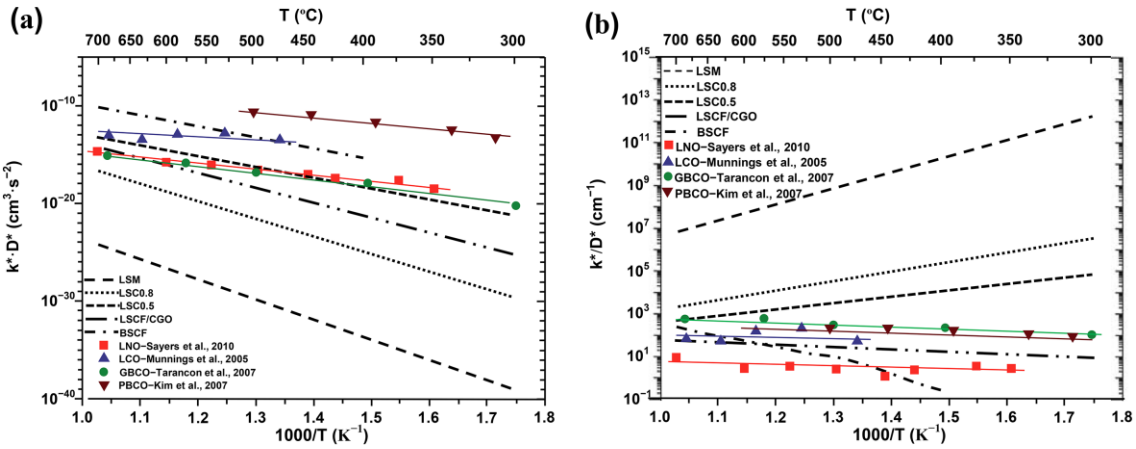

Figure 2. Oxygen tracer diffusion and oxygen surface exchange for different layered oxide cathodes as a function of the temperature: (**a**) k*D*; (**b**) k*/D*. The materials used for comparison have been labeled as follows: $La_{0.8}Sr_{0.2}MnO_{3-\delta}$ (LSM), $La_{0.8}Sr_{0.2}CoO_{3-\delta}$ (LSC0.8), $La_{0.5}Sr_{0.5}CoO_{3-\delta}$ (LSC0.5), $La_{0.6}Sr_{0.4}Co_{0.2}Fe_{0.8}O_{3-\delta}/Ce_{0.8}Gd_{0.2}O_{2-\delta}$ (LSCF/CGO), $Ba_{0.5}Sr_{0.5}Co_{0.8}Fe_{0.2}O_{3-\delta}$ (BSCF), $La_2NiO_{4+\delta}$ (LNO) [50], $La_2CoO_{4+\delta}$ (LCO) [51], $GdBaCo_2O_{5+x}$ (GBCO) [52], and $PrBaCo_2O_{5+x}$ (PBCO) [47] . [Reprinted with permission from Ref. [44]. Copyright 2010, Royal Society of Chemistry].

Numerous experimental and theoretical studies have been undertaken to delve deeper into the oxygen diffusion behaviors in double perovskites [53–71]. Seymour et al. utilized static atomistic simulations based on the Born model to methodically examine the intrinsic defect processes of the double perovskite $LnBaCo_2O_{5.5}$ (Ln = Y, La, Pr, Nd, Sm, Gd, Dy,

Ho, Er, Yb) [53]. Their research indicated that the defect reaction with the lowest energy stemmed from the Ln/Ba antisite disorder energy, which diminishes with decreasing Ln size. This suggests that the ordered structure's primary foundation is the size difference between the Ln and Ba cations [53]. Parfitt et al. combined molecular dynamics with Born model potentials to study the oxygen transport behavior of $GdBaCo_2O_{5+\delta}$ at 900 K [54,55]. They posited that A-site cation ordering, in contrast to its disordered equivalent, can amplify oxygen bulk diffusivity while decreasing transport in the c-axis direction [54,55]. Importantly, the distinctively anisotropic oxygen diffusion in the double perovskite $GdBaCo_2O_{5+\delta}$ takes place exclusively within the [GdO_δ] and adjacent [CoO_2] layers, as illustrated in Figure 3 [54–57]. Shiiba et al. probed the distribution of oxygen vacancies in $GdBaCo_2O_{5+\delta}$ under various oxygen vacancy concentrations ($0 \leq \delta \leq 1$) and temperatures using a fusion of density functional theory and Monte Carlo simulation [57]. Their analysis showed that oxygen vacancies, which function as oxygen ion carriers, are restricted to the [GdO_δ] and neighboring [CoO_2] layers, reinforcing the anisotropic oxygen diffusion mechanism. Seymour et al. performed theoretical investigations on the oxygen transport properties of layered $PrBaCo_2O_{5+\delta}$ at 650 and 1000 °C, employing the MD method [59–62]. These proposed mechanisms for oxygen conducting were later confirmed experimentally via in situ high-temperature neutron powder diffraction and isotope exchange depth profile methods [59–62]. Additionally, it has been shown that $PrBaCo_2O_{5+\delta}$ has a lower energy barrier for oxygen diffusion perpendicular to the c-axis compared to Nd, suggesting enhanced oxygen ion diffusivity with larger Ln sizes [53,59]. Wang et al. detected rapid cobalt redox reactions in epitaxial $LaBaCo_2O_{5+\delta}$ within a temperature bracket of 260–700 °C, intimately tied to the processes of oxygen release and uptake processes [72]. This finding hints at the potential application of these films in SOFC cathodes. Notably, Wang et al. found the cobalt oxidation in the epitaxial thin films to be substantially swifter than the reduction process, denoting a more rapid oxygen uptake compared to the oxygen release (Figure 4) [72]. Bao et al.'s research further revealed a layer-by-layer oxygen transport mechanism in epitaxial double perovskites, specifically $LnBaCo_2O_{5+\delta}$ (Ln = Pr, Er), which likely originates in their intrinsic anisotropic oxygen diffusion properties [73].

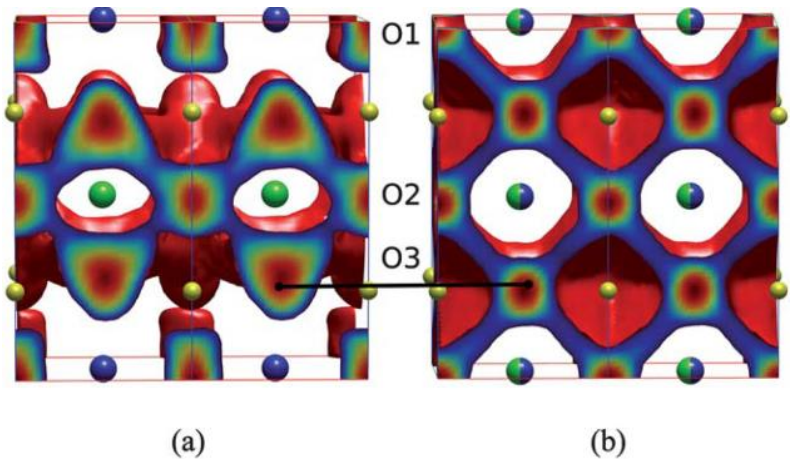

Figure 3. (**a**) Calculated oxygen density profiles showing the oxygen migration pathways for (**a**) ordered and (**b**) disordered $GdBaCo_2O_{5.5}$ for $\delta = 0.5$ at 900 K. [Reprinted with permission from Ref. [54]. Copyright 2011, Royal Society of Chemistry].

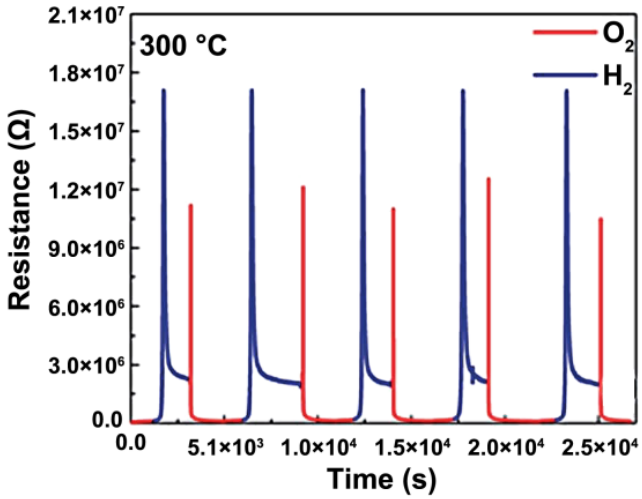

Figure 4. R vs. t curves of redox reactions of the LBCO thin films under the switching flow of a reducing/oxidizing gas flow at 300 °C. [Reprinted with permission from Ref. [72]. Copyright 2014, Royal Society of Chemistry].

$LnBaCo_2O_{5+\delta}$, owing to its exceptionally promising properties, has been extensively studied as a cathode material for SOFCs [34,74–83]. Researchers have undertaken thorough studies into the structural performance, thermal expansion behavior, electrical conductivity, and electrochemical performance of these double perovskites. Studies on ions such as La^{3+}, Pr^{3+}, Nd^{3+}, Sm^{3+}, and Gd^{3+} have shown that these oxides exhibit good chemical compatibility with commonly used electrolytes, including GDC, $La_{0.8}Sr_{0.2}Ga_{0.8}Mg_{0.2}O_{2.8}$ (LSGM), and samarium oxide-doped ceria (SDC), at temperatures below 1000 °C [74–76,84]. After firing $LnBaCo_2O_{5+\delta}$ double perovskites at 850 °C in air for durations ranging from 60 to 100 h, no impurity phases or phase transitions were detected. This finding highlights the remarkable structural stability of these oxides under the standard operating conditions of SOFCs [34,77]. Additionally, the electrical conductivities of $LnBaCo_2O_{5+\delta}$ compounds tend to increase with growth in the size of the Ln ion, leading to a rise in the number of electronic holes created by interstitial oxygen [75,76]. The electrical conductivity values of these materials surpass 100 S cm^{-1} between 100 and 800 °C in air, meeting the electrical conductivity requirements for SOFC cathodes [34,75–77]. What is more, oxides with larger Ln ions exhibit superior electrochemical performance, stemming from enhanced oxygen transport and exchange rates [34,75]. For instance, as the Ln ion shifts from Gd^{3+} to La^{3+}, the maximum power density (PPD) values of SOFCs utilizing these double perovskite cathodes increase from 443 to 516 mW cm^2 [75].

Despite the numerous advantages of $LnBaCo_2O_{5+\delta}$ as a cathode catalyst for SOFCs, there are certain technical challenges that require further improvements. Firstly, enhancing the catalytic activity of these oxides for ORR is paramount. Chen et al. [74] observed that the ASR of $PrBaCo_2O_{5+\delta}$ on SDC electrolytes increases from 0.18 to 5.68 Ω cm^2 as the temperature drops from 650 to 500 °C. Moreover, the PPD of SOFCs utilizing $PrBaCo_2O_{5+\delta}$ as the cathode material decreases from 866 mW cm^2 (at 650 °C) to 115 mW cm^2 (at 500 °C). Secondly, it is essential to minimize the thermal mismatch between these cobalt-based cathode materials and other SOFC components. Kim et al. [75] reported that the thermal expansion coefficients (TECs) of $LnBaCo_2O_{5+\delta}$ double perovskites increase from 16.6 × 10^{-6} K^{-1} (Ln = Gd^{3+}) to 24.3 × 10^{-6} K^{-1} (Ln = Pr^{3+}) with larger Ln sizes at 80–900 °C. Given that the TECs of standard electrolytes for SOFCs, such as GDC, SDC, and LSGM, are around 11 × 10^{-6} K^{-1}, this notable thermal mismatch between $LnBaCo_2O_{5+\delta}$ and the electrolyte could adversely affect fuel cell stability. Thirdly, tuning the physicochemical properties of the surface is essential. The surface physicochemical properties serving as catalysts for the ORR significantly influence cathode performance. Findings by Téllez et al. [79] suggest that the surface composition and morphology of $LnBaCo_2O_{5+\delta}$ (Ln = Pr, Gd) double perovskites

are profoundly influenced by exposure time, temperature, and ambient atmosphere. A quick covering of the electrocatalytic transition metal by inactive Ln^{3+} or Ba^{2+} cations, observed under certain conditions, can be detrimental to the ORR. Therefore, the subsequent sections will provide a comprehensive overview of advancements in studying the physicochemical property attributes of double perovskites and in adjusting the composition and nanostructure of $LnBaCo_2O_{5+\delta}$.

3. Compositional Optimization of $LnBaCo_2O_{5+\delta}$

To enhance the performance of double perovskite-based cathodes, extensive efforts have been made to optimize the composition of $LnBaCo_2O_{5+\delta}$. These modifications involve A-site and B-site doping, or a combination of both, aiming to improve structural stability, enhance chemical compatibility with the electrolyte, increase electrocatalytic activity, and finely tune the TECs (Table 1) [73,85–118]. Marrero-Jerez et al. [85] found that substituting Sr for Ba in $GdBaCo_2O_{5+\delta}$ completely stabilizes the high-temperature tetragonal symmetry even at room temperature. Kim et al. [86] observed improved chemical stability when GDC and LSGM electrolytes are used. Numerous investigations have systematically examined the electrical and electrochemical properties of the $LnBa_{1-x}Sr_xCo_2O_{5+\delta}$ system, with Ln representing La^{3+} [73], Pr^{3+} [87,92], Nd^{3+} [90,91], Sm^{3+} [87–89,112,114], and Gd^{3+} [85–87,111]. Kim et al. [86] demonstrated that the electrical conductivity of $GdBa_{1-x}Sr_xCo_2O_{5+\delta}$ increases with rising Sr content, attributed to increased oxygen content, which is believed to be linked to the difference in A-site cation radii between $(Ba_{1-x}Sr_x)^{2+}$ and Gd^{3+}. Additionally, Subardi et al. [88] found that the double perovskite $SmBa_{0.6}Sr_{0.4}Co_2O_{5+\delta}$ has a relatively high D_{chem} (1.63×10^{-6} cm^2 s^{-1} at 500 °C and 1.41×10^{-5} cm^2 s^{-1} at 700 °C) and a notably low activation energy (E_a = 68.03 kJ mol^{-1}) for oxygen bulk diffusion at 500–700 °C. Jun et al. [89] demonstrated that Sr substitution in $SmBa_{1-x}Sr_xCo_2O_{5+\delta}$ can boost the catalytic activity of double perovskites. For instance, on a GDC electrolyte, the ASR decreases from 0.192 Ω cm^2 (x = 0.00) to 0.138 Ω cm^2 (x = 0.75), and the maximum power density grows from 0.848 to 1.039 W cm^{-2} at 600 °C (Table 1).

Table 1. Typical electrical conductivity, TEC, and ASR values of double perovskites.

	Electrical Conductivity (S cm^{-1})			TEC (10^{-6} K^{-1})	ASR (Ω cm^2)				Refs
	600	700	800		600	700	800	Electrolyte	
$LaBaCo_2O_{5+\delta}$	558	447	355	-	0.195	0.039	0.010	GDC	[93]
$LaBa_{0.9}Co_2O_{5+\delta}$	483	386	306	-	0.118	0.023	0.007	GDC	[93]
$PrBaCo_2O_{5+\delta}$	208	164	128	23.4 (30–900 °C)	0.181	0.038	0.009	GDC	[94]
	212	170	138	24.6 (30–800 °C)	-	0.078		SDC	[100]
$PrBa_{0.92}Co_2O_{5+\delta}$	233	187	146	22.8 (30–900 °C)	0.093	0.024	0.007	GDC	[94]
$PrBa_{0.5}Sr_{0.5}Co_2O_{5+\delta}$	-	-	-	-	0.688	0.154	-	GDC	[87]
$PrBaCoFeO_{5+\delta}$	91	68	62	24.9 (30–800 °C)	-	0.105	-	SDC	[100]
$NdBa_{0.5}Sr_{0.5}Co_2O_{5+\delta}$	695	556	442	-	-	0.139	0.039	LSGM	[90]
	263	204	191	25.2 (100–800 °C)	2.800	0.676	0.086	SDC	[73]
$SmBaCo_2O_{5+\delta}$	560	440	-	-	0.192	-	-	GDC	[89]
$SmBa_{0.5}Sr_{0.5}Co_2O_{5+\delta}$	1000	810	-	-	0.141	-	-	GDC	[89]
	-	-	-	-	0.631	0.092	-	GDC	[87]
$SmBaCoCuO_{5+\delta}$	27	28	31	15.5 (30–850 °C)	-	0.382	0.086	GDC	[107]
$GdBaCo_2O_{5+\delta}$	311	249	196	-	-	-	-	GDC	[85]
	-	-	-	20.0 (30–900 °C)	0.4	-	-	GDC	[104]
	472	374	305	16.6 (80–900 °C)	-	-	-	GDC	[86]
$GdBa_{0.5}Sr_{0.5}Co_2O_{5+\delta}$	591	492	409	-	-	-	-	-	[85]
	-	-	-	-	1.260	0.561	-	GDC	[87]
$GdBa_{0.4}Sr_{0.6}Co_2O_{5+\delta}$	1099	930	591	19.5 (80–900 °C)	-	-	-	GDC	[86]
$GdBaCo_{1.7}Ni_{0.3}O_{5+\delta}$	-	-	-	15.5 (30–900 °C)	0.54	0.297	-	GDC	[104]

The presence of A-site cation deficiency has been found to significantly influence the physical and chemical properties of perovskite oxides, as reported in previous studies [119]. Extensive investigations have been undertaken to understand the effects of Ba^{2+} [93–97,120,121] and Ln^{3+} [122–125] deficiencies on the crystal structure, oxygen content, electrical conductivity, and electrochemical performance of double perovskite $LnBaCo_2O_{5+\delta}$. Pang et al. [94,95] observed that with an increase in Ba deficiency from x = 0.00 (0.181 Ω cm^2) to x = 0.08 (0.093 Ω cm^2) at 600 °C, the ASR value of $PrBa_{1-x}Co_2O_{5+\delta}$

drops by approximately 50%. This indicates a substantial improvement in oxygen catalytic activity associated with A-site deficiency. Dong et al. [98] further revealed that a higher Ba deficiency in $PrBa_{1-x}Co_2O_{5+\delta}$ oxides results in an increased concentration of oxygen vacancies, thus boosting oxygen transport and exchange kinetics. These findings strongly suggest that A-site cation deficiency can enhance the electrochemical performance of double perovskite $LnBaCo_2O_{5+\delta}$.

Ca doping and optimization of the Ln component have been identified as other effective strategies to boost the electrochemical performance of double perovskite cathodes [86,126–153]. Yoo et al. proposed novel cathode materials, such as Ca-doped $NdBaCo_2O_{5+\delta}$, that have ionic radii similar to Nd and demonstrated their impressive structural stability and outstanding electrochemical performance [99]. The ASR of $NdBa_{1-x}Ca_xCo_2O_{5+\delta}$ double perovskites was observed to decrease from 0.091 Ω cm^2 (x = 0.00) to 0.066 Ω cm^2 (x = 0.25) at 600 °C. As illustrated in Figure 5, compared to the Ca-free sample, single cells using $NdBa_{0.75}Ca_{0.25}Co_2O_{5+\delta}$ as the cathode exhibited a significantly higher PPD of 2.114 W cm^{-2} at 600 °C. Moreover, while the power density of the single cell with an $NdBaCo_2O_{5+\delta}$ cathode experienced a decrease of approximately 50%, nearly no degradation in power density was seen for $NdBa_{0.75}Ca_{0.25}Co_2O_{5+\delta}$, highlighting its remarkable stability. This result is believed to correlate with the increased electron affinity of mobile oxygen species in the presence of Ca.

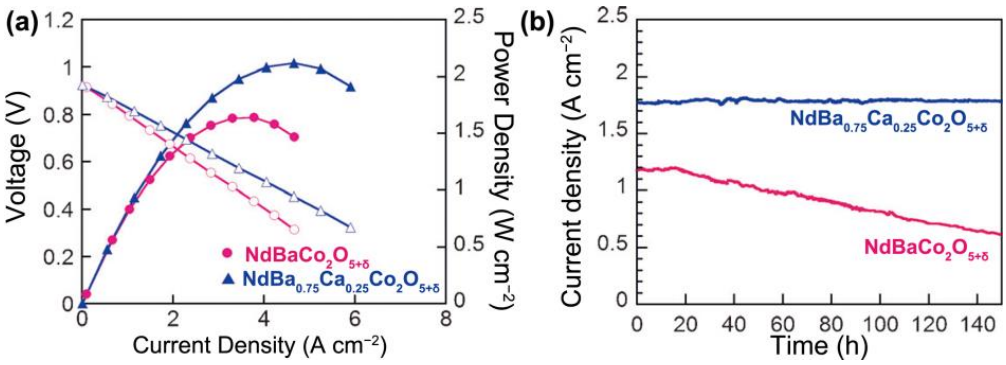

Figure 5. Electrochemical performances and long-term stability data. (**a**) I–V curves and the corresponding power densities of test cells at 600 °C. The solid and hollow circles represent $NdBaCo_2O_{5+\delta}$, while the solid and hollow triangles represent $NdBa_{0.75}Ca_{0.25}Co_2O_{5+\delta}$. (**b**) Long term stability measurement at a constant cell voltage of 0.6 V at 550 °C. [Reprinted with permission from Ref. [99]. Copyright 2014, John Wiley and Sons].

Similar to other cobalt-based cathode materials, $LnBaCo_2O_{5+\delta}$ often displays relatively high TECs, typically ranging from 19 to 25 × 10^{-6} K^{-1} at 80–900 °C. These values are substantially higher than those of conventional electrolytes (10–13 × 10^{-6} K^{-1}) [154] and sealing materials (11–14 × 10^{-6} K^{-1}) [155]. Such differences can lead to significant compatibility issues between the double perovskites and other components of SOFCs during cell fabrication and thermal cycling, potentially causing performance degradation. Besides lattice anharmonic vibrations, the elevated TECs of cobalt-based oxides are mainly attributed to the conversion of smaller Co^{4+} ions to larger Co^{3+} ions at higher temperatures. This is due to the liberation of lattice oxygen upon heating and the spin-state changes of Co^{3+} ions [156,157]. To address these drawbacks, researchers have examined the substitution of cobalt with various elements, including Fe [100–102,158–163], Ni [103,104,164–166], Cu [105–107], Mn [167,168], Zn [169], Zr [170,171], W [172], Sc [173], Mo [174], Ga [175], and Bi [176]. Jo et al. [104] reported that partial substitution of Fe and Cu for Co in $GdBaCo_2O_{5+\delta}$ ($GdBaCo_{2/3}Fe_{2/3}Cu_{2/3}O_{5+\delta}$) can reduce the TECs from 19.9 × 10^{-6} K^{-1} to 14.6 × 10^{-6} K^{-1} at 80–900 °C. Zhao et al. [100] conducted a comprehensive investigation into the impact of Fe content on the physicochemical properties of double perovskite $PrBaCo_2O_{5+\delta}$, discovering a continuous decrease in TECs with higher Fe content. However,

this substitution also led to reduced electrical conductivity, oxygen vacancy concentration, and electrochemical performance compared to the Fe-free compound. For an in-depth exploration of this subject, readers are encouraged to refer to relevant review articles [177].

The ability to incorporate dopants at both the A-site and B-site offers a broader spectrum for customizing double perovskite cathode materials [102,108–110,178–180]. As earlier elaborated, appropriate A-site doping in $LnBaCo_2O_{5+\delta}$, like substituting Ba with Sr or inducing a Ba deficiency, has the potential to enhance electrical conductivity, oxygen bulk diffusivity, surface exchange kinetics, and the oxygen catalytic activity pertinent to ORR [86,89,94,181]. On the other hand, replacing Co with different metal ions, including Fe, Ni, and Cu, has proven to successfully enhance the structural resilience and thermal expansion coefficients, thus improving compatibility with the electrolyte [100,101,103–105]. For instance, Kim et al. [110] deftly adjusted the manganese content in $NdBa_{0.5}Sr_{0.5}Co_{2-x}Mn_xO_{5+\delta}$ to refine its physicochemical attributes as a cathode catalyst for SOFCs. They found that an increase in manganese content led to a decrease in TEC from 20.27×10^{-6} K^{-1} (x = 0.0) to 14.33×10^{-6} K^{-1} (x = 0.5), while maintaining acceptable electrochemical performance. Similarly, Choi et al. [108] documented a robust cathode material, $PrBa_{0.5}Sr_{0.5}Co_{2-x}Fe_xO_{5+\delta}$, which exhibited increased oxygen ion mobility and surface oxygen exchange reactions, superior electrochemical performance (~0.056 Ω cm^{-2} at 600 °C), and strong compatibility and stability with a GDC electrolyte. Persistent optimization of double perovskite composition is essential to uncover innovative cathode materials boasting excellent structural stability, advantageous chemical and thermal compatibility with the electrolyte, adequate electrical conductivities, swift oxygen transport and exchange kinetics, high catalytic ORR activity, and outstanding durability.

4. Nanostructure and Nanoscience of $LnBaCo_2O_{5+\delta}$

Nanostructures offer significantly enhanced surface area-to-volume ratios and expanded interphase and interfacial areas. As such, they have the potential to augment electrochemical reaction sites. Perovskite oxides with nanostructured morphologies have been rigorously studied and employed in solid oxide fuel cells [182–198] as well as other energy-related applications [199–202]. Reducing the operating temperature creates an opportunity to use nanostructured materials, which can sidestep the slow ORR and, in turn, boost the catalytic performance of the cathode [182–198]. Infiltration is a common and straightforward method for developing nanostructured cathode materials tailored for SOFCs [182–184]. A nanostructured cathode material, represented by the formula $SmBa_{0.5}Sr_{0.5}Co_2O_{5+\delta}$, was created by infusing its precursor solution into the porous LSGM framework, followed by calcining at 850 °C. This material showcased commendable electrochemical performance [185]. For instance, it showed an ASR as low as 0.12 Ω cm^2 and a PPD of up to 0.70 W cm^{-2} at 500 °C. Electrospinning, praised for its scalability and precision, was utilized to fabricate a $GdBaCo_2O_{5+\delta}$ cathode material possessing a nanofiber configuration, achieving a comparatively low ASR, approximately 0.10 Ω cm^2 at 700 °C [194].

Ding et al. [185] managed to produce unique needle-like nanospikes of the cathode material $PrBaCo_2O_{5+\delta}$ by applying a discharge voltage of 0.1 V to the anode-supported single cell, arranged as NiO-$Sm_{0.2}Ce_{0.8}O_{1.9}$/$Sm_{0.2}Ce_{0.8}O_{1.9}$/$PrBaCo_2O_{5+\delta}$, and then firing the $PrBaCo_2O_{5+\delta}$ cathode slurry at 450 °C. As illustrated in Figure 6, these nanospikes, with an average diameter of 20 nm and lengths spanning from tens to hundreds of nanometers, are uniformly distributed along the pore boundaries of the porous cathode. For the single cell that used the nanospikes $PrBaCo_2O_{5+\delta}$ as the cathode, exceptionally high maximum power densities of 1.453 W cm^{-2} at 550 °C and 1.044 W cm^{-2} at 500 °C, coupled with excellent endurance, were recorded.

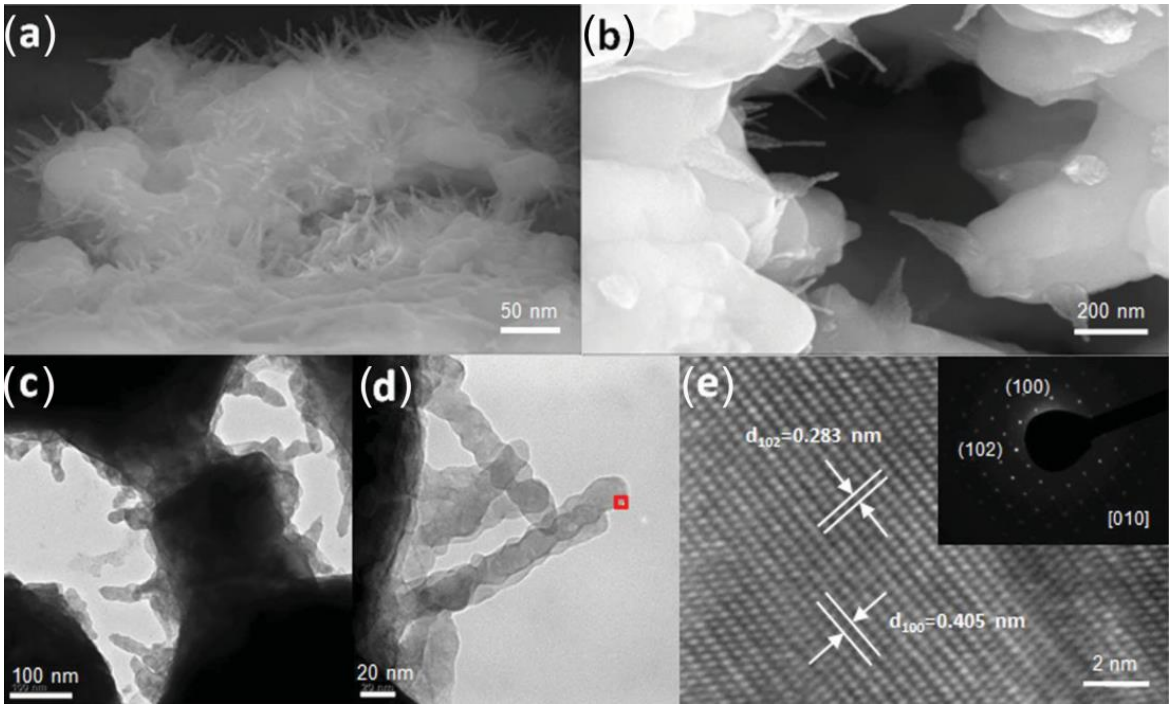

Figure 6. (**a**,**b**) Cross-sectional view (field emission SEM image) of cathode–electrolyte interface at different locations. (**c**,**d**) TEM view of nanospikes growing from $PrBaCo_2O_{5+\delta}$ bulk. (**e**) HRTEM lattice fringe image of a nanospike tip (boxed area in (**d**)), and SAED pattern along [010] zone axis (insert). [Reprinted with permission from Ref. [185]. Copyright 2014, John Wiley and Sons].

The fabrication of double perovskites in a thin-film architecture not only facilitates fundamental studies to evaluate inherent properties of materials [73,183,203,204] but also illuminates a new avenue for the development of high-performing cathode materials [72,186,188]. The influence of orientations on the electrochemical performance of double perovskites was appraised by Gao et al. [186]. They produced $PrBaCo_2O_{5+\delta}$ thin films with different orientations, including (110), (001), and (111), using pulsed laser deposition. The thin film with the (111) orientation showed superior performance, achieving an ASR of 0.302 Ω cm^2 at 600 °C. Liu et al. [187,188] fabricated symmetric half-cells by coupling single-crystal, highly epitaxial $LnBaCo_2O_{5+\delta}$ (Ln = Pr, La) thin-film cathodes with $Gd_{0.8}Ce_{0.2}O_2$:$Y_{0.08}Zr_{0.92}O_2$ electrolytes and subsequently characterized their oxygen surface exchange and catalytic activity. For instance, the symmetric half-cell featuring the epitaxial $LaBaCo_2O_{5+\delta}$ thin film displayed remarkable properties, such as an impressively fast surface exchange rate of 0.017 cm s^{-1} at 600 °C and an exceptionally low activation energy value of 0.49 eV. These outcomes might be ascribed to the structural entropy arising from the nano-ordered oxygen vacancy framework.

5. Conclusions and Outlook

This manuscript addresses the development of novel strategies concerning the double perovskites $LnBaCo_2O_{5+\delta}$, which possess rapid oxygen bulk diffusivity and a high surface exchange rate. These parameters serve as the cornerstone for achieving advanced catalytic activity for the ORR; hence, they are essential for cathode materials operating within intermediate-to-low temperature SOFCs. The discourse encompasses physicochemical characteristics, compositional fine-tuning, and the implementation of nanostructure and nanoscience within double perovskites. Potential research focuses for advancing high-performance double perovskite-based cathode materials include:

(1) Surface Chemistry of $LnBaCo_2O_{5+\delta}$ Under Operating Conditions

The surface physicochemical properties of double perovskite $LnBaCo_2O_{5+\delta}$, as catalysts for the ORR, are essential for their practical application. Téllez et al. [79] characterized the surface chemistry evolution in double perovskite $LnBaCo_2O_{5+\delta}$ (Ln = Pr, Gd) using low-energy ion scattering, spectrometry, and atomic force microscopy. They found that the surface composition and morphology of $LnBaCo_2O_{5+\delta}$ (Ln = Pr, Gd) are sensitive to their ambient environment. Inactive Ba-rich layers emerged on the double perovskite surface following annealing, adversely affecting oxygen surface exchange processes and, subsequently, the electrochemical performance. Druce et al. [205] observed a similar surface termination and subsurface restructuring for $GdBaCo_2O_{5+\delta}$. According to Lee et al. [206], the segregation originates from the dopant's elastic and electrostatic interactions with the host lattice. A slight size mismatch between the dopant and host cations could reduce this segregation, promoting a more stable cathode surface [205–215]. Nonetheless, the majority of research on the surface microstructure of double perovskite cathodes relies on basic sintering processes in the air, which differs significantly from actual battery operating conditions. Hence, guidance for the practical use of double perovskites remains limited. Investigating surface microstructure evolution under the SOFCs' actual operational conditions and creating targeted enhancement strategies offer a promising path for practical deployment of these cathode materials.

(2) Microstructure of $LnBaCo_2O_{5+\delta}$ Cathode Materials

The structural design of double perovskite metal oxides offers advantages for their use in the cathodic parts of SOFCs. Nevertheless, in practical applications, these double perovskites often present as polycrystalline particles. It is believed that features such as grain orientation, microstructure, lattice strain, and chemical imperfections strongly influence their catalytic activity [72,73,183,186,188,189,193,203,216–218]. Consequently, a comprehensive study on the microstructure of these double perovskite particles is crucial for high-performance SOFC cathodes. For instance, Fu et al. found that a dual-phase cathode containing both double perovskite $PrBa(Co_{1-x}Fe_x)_2O_{5+\delta}$ and simple perovskite $Pr_{0.5}Ba_{0.5}Co_{1-x}Fe_xO_{3-\delta}$ significantly enhanced the cathode's oxygen catalysis [193]. Likewise, Pang et al. engineered a biomimetic ceramic catalyst resembling tree leaves, incorporating $Ce_{0.9}Gd_{0.1}O_{1.95}$ "epidermis" and "veins" externally and inside the bulk of the $PrBaCo_2O_{5+\delta}$ [189]. This unique design substantially improved cell performance, inducing a 79% rise in the cell's output power density, reversing the rapid decline trend, yielding a 23% power density gain in the initial 20 h, and stabilizing at 0.91 W cm^{-2} (at 750 °C and 0.7 V) [189].

Author Contributions: Conceptualization, S.P.; methodology, F.Z.; writing—original draft preparation, F.Z.; writing—review and editing, S.P.; visualization, F.Z.; supervision, S.P.; project administration, S.P.; funding acquisition, S.P. All authors have read and agreed to the published version of the manuscript.

Funding: This research was funded by the National Natural Science Foundation of China (Grant No. U2032157) and the Natural Science Foundation of Jiangsu Province (Grant No. BK20201425).

Data Availability Statement: No new data were created.

Conflicts of Interest: The authors declare no conflict of interest. The funders had no role in the design of the study; in the collection, analyses, or interpretation of data; in the writing of the manuscript; or in the decision to publish the results.

References

1. Wachsman, E.D.; Lee, K.T. Lowering the temperature of solid oxide fuel cells. *Science* **2011**, *334*, 935–939. [CrossRef] [PubMed]
2. Wachsman, E.; Ishihara, T.; Kilner, J. Low-temperature of solid-oxide fuel cells. *MRS Bulletin* **2014**, *39*, 773–779. [CrossRef]
3. Steele, B.C.H.; Heinzel, A. Materials for fuel-cell technologies. *Nature* **2001**, *414*, 345–352. [CrossRef] [PubMed]
4. Xia, C.; Lang, Y.; Meng, G. Recent advances to the development of low-temperature solid oxide fuel cells. *Fuel Cells* **2004**, *4*, 41–47. [CrossRef]
5. Xia, C.R.; Xia, M.L. Novel cathodes for low-temperature solid oxide fuel cells. *Adv. Mater.* **2002**, *14*, 521–523. [CrossRef]
6. Kilner, J.A.; Burriel, M. Intermediate-temperature solid-oxide fuel cells. *Annu. Rev. Mater. Res.* **2014**, *44*, 365–393. [CrossRef]

7. Zhou, W.; Sunarso, J.; Zhao, M.; Liang, F.; Klande, T.; Feldhoff, A. A highly active perovskites electrode for the oxygen reduction reaction below 600 °C. *Angew. Chem. Int. Ed.* **2013**, *52*, 14036–14040. [CrossRef]
8. Jiang, S.P. Development of lanthanum strontium manganite perovskite cathode materials of solid oxide fuel cells: A review. *J. Mater. Sci.* **2008**, *43*, 6799–6833. [CrossRef]
9. Adler, S.B. Factors governing oxygen reduction in solid oxide fuel cell cathodes. *Chem. Rev.* **2004**, *104*, 4791–4843. [CrossRef]
10. Adler, S.B. Mechanism and kinetics of oxygen reduction on porous $La_{1-x}Sr_xCoO_{3-\delta}$ electrodes. *Solid State Ionics* **1998**, *111*, 125–134. [CrossRef]
11. Adler, S.B.; Lane, J.A.; Steele, B.C.H. Electrode kinetics of porous mixed-conducting oxygen electrodes. *J. Electrochem. Soc.* **1996**, *143*, 3554–3564. [CrossRef]
12. Hwang, H.J.; Moon, J.-W.; Lee, S.; Lee, E.A. Electrochemical performance of LSCF-based composite cathodes for intermediate temperature SOFCs. *J. Power Sources* **2005**, *145*, 243–248. [CrossRef]
13. Pang, S.L.; Jiang, X.N.; Li, X.N.; Wang, Q.; Su, Z.X. A comparative study of electrochemical performance of $La_{0.5}Ba_{0.5}CoO_{3-\delta}$ and $La_{0.5}Ba_{0.5}CoO_{3-\delta}$-$Gd_{0.1}Ce_{0.9}O_{1.95}$ cathodes. *Int. J. Hydrogen Energy* **2012**, *37*, 2157–2165. [CrossRef]
14. Steele, B.C.H. Appraisal of $Ce_{1-y}Gd_yO_{2-y/2}$ electrolytes for IT-SOFC operation at 500 °C. *Solid State Ionics* **2000**, *129*, 95–110. [CrossRef]
15. Bao, S.; Pang, S.; Wang, W.; Chen, J.; Chen, M.; Ma, J.; Nan, C.-W.; Chen, C. Ca doping effect on the magnetic and electronic transport properties in double perovskite $PrBaCo_2O_{5+\delta}$ films. *Appl. Phys. Lett.* **2017**, *111*, 232406. [CrossRef]
16. Wu, J.; Guzman, R.; Bao, S.; Zhang, Y.; Chen, Y.; Shen, S.; Yu, P.; Nan, C.-W.; Zhou, W.; Chen, C.; et al. Mosaic growth induced magnetic anisotropy in double perovskite $PrBaCo_2O_{5+\delta}$ thin films. *Acta Materialia* **2022**, *234*, 118040. [CrossRef]
17. Kudyakova, V.S.; Shalamova, A.M.; Politov, B.V.; Suntsov, A.Y. Specific interrelations of magnetic, thermodynamic and structural properties in highly non-stoichiometric $PrBaMnFeO_{6-\delta}$ double perovskite. *J. Alloys Compd.* **2021**, *886*, 161133. [CrossRef]
18. Choi, S.; Kucharczyk, C.J.; Liang, Y.; Zhang, X.; Takeuchi, I.; Ji, H.-I.; Haile, S.M. Exceptional power density and stability at intermediate temperatures in protonic ceramic fuel cells. *Nat. Energy* **2018**, *3*, 202–210. [CrossRef]
19. Wang, N.; Tang, C.; Du, L.; Zhu, R.; Xing, L.; Song, Z.; Yuan, B.; Zhao, L.; Aoki, Y.; Ye, S. Advanced cathode materials for protonic ceramic fuel cells: Recent progress and future perspectives. *Adv. Energy Mater.* **2022**, *12*, 2201882. [CrossRef]
20. Teketel, B.S.; Beshiwork, B.A.; Luo, X.; Tian, D.; Zhu, S.; Desta, H.G.; Yang, Q.; Chen, Y.; Lin, B. A-site doping enabled higher-oxygen-vacancy cobalt-free layered perovskite cathode for higher-performing protonic ceramic fuel cells. *Ceram. Int.* **2022**, *48*, 37232–37241. [CrossRef]
21. Islam, M.S.; Wang, S.; Nolan, A.M.; Mo, Y. First-principles computational design and discovery of novel double-perovskite proton conductors. *Chem. Mater.* **2021**, *33*, 8278–8288. [CrossRef]
22. Cao, J.; Jia, Y.; Shao, Z. Perovskites for protonic ceramic fuel cells: A review. *Energy Environ. Sci.* **2022**, *15*, 2200–2232. [CrossRef]
23. Teketel, B.S.; Beshiwork, B.A.; Tian, D.; Zhu, S.; Desta, H.G.; Kashif, K.; Chen, Y.; Lin, B. Promoted performance of layered perovskite $PrBaFe_2O_{5+\delta}$ cathode for protonic ceramic fuel cells by Zn doping. *Catalysts* **2022**, *12*, 488. [CrossRef]
24. Zhang, H.; Xu, K.; He, F.; Zhou, Y.; Sasaki, K.; Zhao, B.; Choi, Y.; Liu, M.; Chen, Y. Surface regulating of a double-perovskite electrode for protonic ceramic fuel cells to enhance oxygen reduction activity and contaminants poisoning tolerance. *Adv. Energy Mater.* **2022**, *12*, 2200761. [CrossRef]
25. Malyshkin, D.; Novikov, A.; Ivanov, I.; Sereda, V.; Tsvetkov, D.; Zuev, A. The origin of triple conductivity and water uptake in layered double perovskites: A case study on lanthanum-substituted $GdBaCo_2O_{6-\delta}$. *J. Alloys Compd.* **2020**, *845*, 156309. [CrossRef]
26. Kim, B.-J.; Fabbri, E.; Castelli, I.E.; Borlaf, M.; Graule, T.; Nachtegaal, M.; Schmidt, T.J. Fe-doping in double perovskite $PrBaCo_{2(1-x)}Fe_{2x}O_{6-\delta}$: Insights into structural and electronic effects to enhance oxygen evolution catalyst stability. *Catalysts* **2019**, *9*, 263. [CrossRef]
27. Xing, L.; Xia, T.; Li, Q.; Zhao, H.; Sun, L.; Huo, L.-H. High-Performance and CO_2-durable composite cathodes toward electrocatalytic oxygen reduction: $Ce_{0.8}Sm_{0.2}O_{1.9}$ Nanoparticle-decorated double perovskite $EuBa_{0.5}Sr_{0.5}Co_2O_{5+\delta}$. *ACS Sust. Chem. Eng.* **2019**, *7*, 17907–17918. [CrossRef]
28. Baral, A.K.; Sankar, K.V.; Matatyaho, A.; Kushnir, G.; Tsur, Y. Tri-functional double perovskite oxide catalysts for fuel cells and electrolyzers. *ChemSusChem* **2020**, *13*, 5671–5682. [CrossRef]
29. Shin, T.H.; Myung, J.-H.; Verbraeken, M.; Kim, G.; Irvine, J.T.S. Oxygen deficient layered double perovskite as an active cathode for CO_2 electrolysis using a solid oxide conductor. *Faraday Discuss.* **2015**, *182*, 227. [CrossRef]
30. Wang, H.; Enriquez, E.; Collins, G.; Ma, C.; Liu, M.; Zhang, Y.; Dong, C.; Chen, C. Anomalous redox properties and ultrafast chemical sensing behavior of double perovskite $CaBaCo_2O_{5+\delta}$ thin films. *J. Materiomics* **2015**, *1*, 113–117. [CrossRef]
31. Luo, Y.; Xu, X.; Xia, Y.; Pang, S.; Xu, F.; Whangbo, M.-H.; Sun, L.; Chen, C. Anomaly negative resistance phenomena in highly epitaxial $PrBa_{0.7}Ca_{0.3}Co_2O_{5+\delta}$ thin films induced from superfast redox reactions. *Catalysts* **2021**, *11*, 1441. [CrossRef]
32. Bao, S.; Ma, C.; Chen, G.; Xu, X.; Enriquez, E.; Chen, C.; Zhang, Y.; Bettis, J.L.; Whangbo, M.-H.; Dong, C.; et al. Ultrafast atomic layer-by-layer oxygen vacancy-exchange diffusion in double-perovskite $LnBaCo_2O_{5.5+\delta}$ thin films. *Sci. Rep.* **2014**, *4*, 4726. [CrossRef] [PubMed]
33. Ivanov, I.L.; Zakiryanov, P.O.; Sereda, V.V.; Mazurin, M.O.; Malyshkin, D.A.; Zuev, A.Y.; Tsvetkov, D.S. Nonstoichiometry, Defect chemistry and oxygen transport in Fe-doped layered double perovskite cobaltite $PrBaCo_{2-x}Fe_xO_{6-\delta}$ (x = 0–0.6) membrane materials. *Membranes* **2022**, *12*, 1200. [CrossRef] [PubMed]

34. Zhang, K.; Ge, L.; Ran, R.; Shao, Z.; Liu, S. Synthesis, characterization and evaluation of cation-ordered $LnBaCo_2O_{5+\delta}$ as materials of oxygen permeation membranes and cathodes of SOFCs. *Acta Mater.* **2008**, *56*, 4876–4889. [CrossRef]
35. Yagovitin, R.E.; Tsvetkov, D.S.; Ivanov, I.L.; Malyshkin, D.A.; Sereda, V.V.; Zuev, A.Y. Thermodynamics of Formation and Disordering of $YBaCo_2O_{6-\delta}$ Double Perovskite as a Base for Novel Dense Ceramic Membrane Materials. *Membranes* **2023**, *13*, 10. [CrossRef]
36. Zhao, B.; Zhang, L.; Zhen, D.; Yoo, S.; Ding, Y.; Chen, D.; Chen, Y.; Zhang, Q.; Doyle, B.; Xiong, X.; et al. A tailored double perovskite nanofiber catalyst enables ultrafast oxygen evolution. *Nat. Commun.* **2017**, *8*, 14586. [CrossRef]
37. Hua, B.; Zhang, Y.-Q.; Yan, N.; Li, M.; Sun, Y.-F.; Chen, J.; Li, J.; Luo, J.-L. The excellence of both worlds: Developing effective double perovskite oxide catalyst of oxygen reduction reaction for room and elevated temperature applications. *Adv. Funct. Mater.* **2016**, *26*, 4106–4112. [CrossRef]
38. Fang, F.; Feng, N.; Zhao, P.; Chen, C.; Li, X.; Meng, J.; Liu, G.; Chen, L.; Wan, H.; Guan, G. In situ exsolution of Co/CoO_x core-shell nanoparticles on double perovskite porous nanotubular webs: A synergistically active catalyst for soot efficient oxidation. *Chem. Eng. J.* **2019**, *372*, 752–764. [CrossRef]
39. Wang, Z.; Liu, Y.; Chen, Y.; Yang, L.; Wang, Y.; Wei, M. A-site cation-ordered double perovskite $PrBaCo_2O_{5+\delta}$ oxide as an anion-inserted pseudocapacitor electrode with outstanding stability. *J. Alloys Compd.* **2019**, *810*, 151830. [CrossRef]
40. Zhang, R.; Hu, S.; Lu, C.; Xu, Z. Bandgap engineering of $Gd_{0.8}Ca_{0.2}BaCo_2O_{5+\delta}$ double perovskite for photocatalysis applications. *Ceram. Int.* **2018**, *44*, 15483–15489. [CrossRef]
41. Lu, Y.; Dai, T.; Lu, C.; Cao, C.; Zhang, W.; Xu, W.; Min, H.; Yang, X. Fabrication of doped $SmBaCo_2O_{5+\delta}$ double perovskites for enhanced solar driven interfacial evaporation. *Ceram. Int.* **2019**, *45*, 24903–24908. [CrossRef]
42. Lu, Y.; Zhang, R.; Wei, L.; Lu, C.; Ni, Y.; Xu, Z. Specific features of spectral and electrical properties of double-perovskite $LnBaCo_2O_{5+\delta}$ (Ln=lanthanides) under solar irradiation. *Ceram. Int.* **2017**, *43*, 1186–1192. [CrossRef]
43. Kim, J.-H.; Manthiram, A. Layered $LnBaCo_2O_{5+\delta}$ perovskite cathodes for solid oxide fuel cells: An overview and perspective. *J. Mater. Chem. A* **2015**, *3*, 24195–24210. [CrossRef]
44. Tarancón, A.; Burriel, M.; Santiso, J.; Skinner, S.J.; Kilner, J.A. Advances in layered oxide cathodes for intermediate temperature solid oxide fuel cells. *J. Mater. Chem.* **2010**, *20*, 3799–3813. [CrossRef]
45. Taskin, A.A.; Lavrov, A.N.; Ando, Y. Achieving fast oxygen diffusion in perovskites by cation ordering. *Appl. Phys. Lett.* **2005**, *86*, 091910. [CrossRef]
46. Taskin, A.A.; Lavrov, A.N.; Ando, Y. Transport and magnetic properties of $GdBaCo_2O_{5+\delta}$ single crystals: A cobalt oxide with square-lattice CoO_2 planes over a wide range of electron and hole doping. *Phys. Rev. B* **2005**, *71*, 134414. [CrossRef]
47. Kim, G.; Wang, S.; Jacobson, A.J.; Reimus, L.; Brodersen, P.; Mims, C.A. Rapid oxygen ion diffusion and surface exchange kinetics in $PrBaCo_2O_{5+x}$ with a perovskite related structure and ordered A cations. *J. Mater. Chem.* **2007**, *17*, 2500–2505. [CrossRef]
48. Kim, G.; Wang, S.; Jacobson, A.J.; Yang, Z.; Donner, W.; Chen, C.L.; Reimus, L.; Brodersen, P.; Mims, C.A. Oxygen exchange kinetics of epitaxial $PrBaCo_2O_{5+\delta}$ thin films. *Appl. Phys. Lett.* **2006**, *88*, 024103. [CrossRef]
49. Tsvetkov, D.S.; Ananjev, M.V.; Eremin, V.A.; Zuev, A.Y.; Kurumchin, E.K. Oxygen nonstoichiometry, defect structure and oxygen diffusion in the double perovskite $GdBaCo_2O_{6-\delta}$. *Dalton Trans.* **2014**, *43*, 15937–15943. [CrossRef]
50. Sayers, R.; De Souza, R.A.; Kilner, J.A.; Skinner, S.J. Low temperature diffusion and oxygen stoichiometry in lanthanum nickelate. *Solid State Ionics* **2010**, *181*, 386–391. [CrossRef]
51. Munnings, C.N.; Skinner, S.J.; Amow, G. Whitfield, P.S;. Davidson, I.J. Oxygen transport in the $La_2Ni_{1-x}Co_xO_{4+\delta}$ system. *Solid State Ionics* **2005**, *176*, 1895–1901. [CrossRef]
52. Tarancón, A.; Morata, A.; Dezanneau, G.; Skinner, S.J.; Kilner, J.A.; Estradé, S.; Hernández-Ramírez, F.; Peiró, F.; Morante, J.R. $GdBaCo_2O_{5+x}$ layered perovskite as an intermediate temperature solid oxide fuel cell cathode. *J. Power Sources* **2007**, *174*, 255–263. [CrossRef]
53. Seymour, I.D.; Chroneos, A.; Kilner, J.A.; Grimes, R.W. Defect processes in orthorhombic $LnBaCo_2O_{5.5}$ double perovskites. *Phys. Chem. Chem. Phys.* **2011**, *13*, 15305–15310. [CrossRef] [PubMed]
54. Parfitt, D.; Chroneos, A.; Tarancón, A.; Kilner, J.A. Oxygen ion diffusion in cation ordered/disordered $GdBaCo_2O_{5+\delta}$. *J. Mater. Chem.* **2011**, *21*, 2183–2186. [CrossRef]
55. Tarancón, A.; Chroneos, A.; Parfitt, D.; Kilner, J. Oxygen diffusion in ordered/disordered double perovskites. *Ecs Trans.* **2011**, *35*, 1151–1154. [CrossRef]
56. Hermet, J.; Geneste, G.; Dezanneau, G. Molecular dynamics simulations of oxygen diffusion in $GdBaCo_2O_{5.5}$. *Appl. Phys. Lett.* **2010**, *97*, 174102. [CrossRef]
57. Shiiba, H.; Nakayama, M.; Kasuga, T.; Grimes, R.W.; Kilner, J.A. Calculation of arrangement of oxygen ions and vacancies in double perovskite $GdBaCo_2O_{5+\delta}$ by first-principles DFT with monte carlo simulations. *Phys. Chem. Chem. Phys.* **2013**, *15*, 10494–10499. [CrossRef]
58. Zapata, J.; Burriel, M.; Carcía, P.; Kilner, J.A.; Santiso, J. Anisotropic O^{18} tracer diffusion in epitaxial films of $GdBaCo_2O_{5+\delta}$ cathode material with different orientations. *J. Mater. Chem. A* **2013**, *1*, 7408–7414. [CrossRef]
59. Seymour, I.D.; Tarancón, A.; Chroneos, A.; Parfitt, D.; Kilner, J.A.; Grimes, R.W. Anisotropic oxygen diffusion in $PrBaCo_2O_{5.5}$ double perovskites. *Solid State Ionics* **2012**, *216*, 41–43. [CrossRef]
60. Burriel, M.; Peña-Martínez, J.; Chater, R.J.; Fearn, S.; Berenov, A.V.; Skinner, S.J.; Kilner, J.A. Anisotropic oxygen ion diffusion in layered $PrBaCo_2O_{5+\delta}$. *Chem. Mater.* **2012**, *24*, 613–621. [CrossRef]

61. Chen, Y.-C.; Yashima, M.; Peña-Martínez, J.; Kilner, J.A. Experimental visualization of the diffusional pathway of oxide ions in a layered perovskite-type cobaltite $PrBaCo_2O_{5+\delta}$. *Chem. Mater.* **2013**, *25*, 2638–2641. [CrossRef]
62. Cox-Galhotra, R.A.; Huq, A.; Hodges, J.P.; Yu, C.; Wang, X.; Gong, W.; Jacobson, A.J.; McIntosh, S. An in-situ neutron diffraction study of the crystal structure of $PrBaCo_2O_{5+\delta}$ at high temperature and controlled oxygen partial pressure. *Solid State Ionics* **2013**, *249–250*, 34–40. [CrossRef]
63. Hu, Y.; Hernandez, O.; Broux, T.; Bahout, M.; Hermet, J.; Ottochian, A.; Ritter, C.; Geneste, G.; Dezanneau, G. Oxygen diffusion mechanism in the mixed ion-electron conductor $NdBaCo_2O_{5+x}$. *J. Mater. Chem.* **2012**, *22*, 18744–18747. [CrossRef]
64. Cox-Galhotra, R.A.; Huq, A.; Hodges, J.P.; Kim, J.-H.; Yu, C.; Wang, X.; Jacobson, A.J.; Mcintosh, S. Visualizing oxygen anion transport pathways in $NdBaCo_2O_{5+\delta}$ by in situ neutron diffraction. *J. Mater. Chem.* **2013**, *1*, 3091–3100. [CrossRef]
65. Hermet, J.; Dupé, B.; Dezanneau, G. Simulations of $REBaCo_2O_{5.5}$ (RE = Gd, La, Y) cathode materials through energy minimization and molecular dynamics. *Solid State Ionics* **2012**, *216*, 50–53. [CrossRef]
66. Tsvetkov, D.S.; Sereda, V.V.; Zuev, A.Y. Defect structure and charge transfer in the double perovskite $GdBaCo_2O_{6-\delta}$. *Solid State Ionics* **2011**, *192*, 215–219. [CrossRef]
67. Bernuy-Lopez, C.; Høydalsvik, K.; Einarsrud, M.-A.; Grande, T. Effect of A-site cation ordering on chemical stability, oxygen stoichiometry and electrical conductivity in layered $LaBaCo_2O_5$ double perovskite. *Materials* **2016**, *9*, 154. [CrossRef]
68. Anjum, U.; Khan, T.S.; Agarwal, M.; Haider, M.A. Identifying the origin of the limiting process in a double perovskite $PrBa_{0.5}Sr_{0.5}Co_{1.5}Fe_{0.5}O_{5+\delta}$ Thin-film electrode for solid oxide fuel cells. *ACS Appl. Mater. Interfaces* **2019**, *11*, 25243–25253. [CrossRef]
69. Tsvetkov, D.S.; Sereda, V.V.; Zuev, A.Y. Oxygen nonstoichiometry and defect structure of the double perovskite $GdBaCo_2O_{6-\delta}$. *Solid State Ionics* **2010**, *180*, 1620–1625. [CrossRef]
70. Pang, S.; Wang, W.; Su, Y.; Shen, X.; Wang, Y.; Xu, K.; Chen, C. Synergistic effect of A-site cation ordered-disordered perovskite as a cathode material for intermediate temperature solid oxide fuel cells. *J. Electrochem. Soc.* **2017**, *164*, F775–F780. [CrossRef]
71. Zhou, Y.; Lü, Z.; Xu, S.; Wei, B.; Xu, D.; Yang, Z. The electronic structure and the oxygen adsorption at BaO terminated surface of $GdBaCo_2O_{5.5}$: A first principles study. *Solid State Commun.* **2020**, *311*, 113871. [CrossRef]
72. Wang, H.B.; Bao, S.Y.; Liu, J.; Collins, G.; Ma, C.R.; Liu, M.; Chen, C.L.; Dong, C.; Whangbo, M.-H.; Guo, H.M.; et al. Ultrafast chemical dynamic behavior in highly epitaxial $LaBaCo_2O_{5+\delta}$ thin films. *J. Mater. Chem. C* **2014**, *2*, 5660–5666. [CrossRef]
73. Subardi, A.; Liao, K.Y.; Fu, Y.P. Oxygen transport, thermal and electrochemical properties of $NdBa_{0.5}Sr_{0.5}Co_2O_{5+\delta}$ cathode for SOFCs. *J. Eur. Ceram. Soc.* **2019**, *39*, 30–40. [CrossRef]
74. Chen, D.J.; Ran, R.; Zhang, K.; Wang, J.; Shao, Z.P. Intermediate-temperature electrochemical performance of a polycrystalline $PrBaCo_2O_{5+\delta}$ cathode on samarium-doped ceria electrolyte. *J. Power Sources* **2009**, *188*, 96–105. [CrossRef]
75. Kim, J.-H.; Manthiram, A. $LnBaCo_2O_{5+\delta}$ oxides as cathodes for intermediate-temperature solid oxide fuel cells. *J. Electrochem. Soc.* **2008**, *155*, B385–B390. [CrossRef]
76. Pang, S.L.; Jiang, X.N.; Li, X.N.; Su, Z.X.; Xu, H.X.; Xu, Q.L.; Chen, C.L. Characterization of cation-ordered perovskite oxide $LaBaCo_2O_{5+\delta}$ as cathode for intermediate-temperature solid oxide fuel cells. *Int. J. Hydrogen Energy* **2012**, *37*, 6836–6843. [CrossRef]
77. Pang, S.L.; Jiang, X.N.; Wang, Q.X.N.; Zhang, Q.Y. Structural stability and high-temperature electrical properties of cation-oredered/disordered perovskite LaBaCoO. *Mater. Chem. Phys.* **2012**, *131*, 642–646. [CrossRef]
78. Chen, D.J.; Ran, R.; Shao, Z.P. Effect of firing temperature on the microstructure and performance of $PrBaCo_2O_{5+\delta}$ cathodes on $Sm_{0.2}Ce_{0.8}O_{1.9}$ electrolytes fabricated by spray deposition-firing processes. *J. Power Sources* **2010**, *195*, 4667–4675. [CrossRef]
79. Téllez, H.; Druce, J.; Ju, Y.-W.; Kilner, J.; Ishihara, T. Surface chemistry evolution in $LnBaCo_2O_{5+\delta}$ double perovskites for oxygen electrodes. *Int. J. Hydrogen Energy* **2014**, *39*, 20856–20863. [CrossRef]
80. Muñoz-Gil, D.; Pérez-Coll, D.; Peña-Martínez, J.; Garcia-Martín, S. New insights into the $GdBaCo_2O_{5+\delta}$ material: Crystal structure, electrical and electrochemical properties. *J. Power Sources* **2014**, *263*, 90–97. [CrossRef]
81. Ishizawa, N.; Asaka, T.; Kudo, T.; Fukuda, K.; Yasuhara, A.; Abe, N.; Arima, T. Structural evolution of $GdBaCo_2O_{5+\delta}$ ($\delta = 7/18$) at elevated temperatures. *Chem. Mater.* **2014**, *26*, 6503–6517. [CrossRef]
82. Aksenova, T.V.; Gavrilova, L.Y.; Yaremchenko, A.A.; Cherepanov, V.A.; Kharton, V.V. Oxygen nonstoichiometry, thermal expansion and high-temperature electrical properties of layered $NdBaCo_2O_{5+\delta}$ and $SmBaCo_2O_{5+\delta}$. *Mater. Res. Bull.* **2010**, *45*, 1288–1292. [CrossRef]
83. Shi, Z.; Xia, T.; Meng, F.; Wang, J.; Lian, J.; Zhao, H.; Bassat, J.-M.; Grenier, J.-C.; Meng, J. A layered perovskite $EuBaCo_2O_{5+\delta}$ for intermediate-temperature solid oxide fuel cell cathode. *Fuel Cells* **2013**, *14*, 979–990. [CrossRef]
84. Tsvetkov, D.; Tsvetkova, N.; Ivanov, I.; Malyshkin, D.; Sereda, V.; Zuev, A. $PrBaCo_2O_{6-\delta}$-$Ce_{0.8}Sm_{0.2}O_{1.9}$ composite cathodes for intermediate-temperature solid oxide fuel cells: Stability and cation interdiffusion. *Energies* **2019**, *12*, 417. [CrossRef]
85. Marrero-Jerez, J.; Peña-Martínez, J.; Nñez, P. Study of the oxygen desorption from $GdBa_{1-x}Sr_xCo_2O_{5+\delta}$ (x = 0, 0.25, 0.5 and 1): Effect of the Sr-content on the oxidation state of cobalt ions. *J. Alloys Compd.* **2014**, *606*, 269–272. [CrossRef]
86. Kim, J.-H.; Prado, F.; Manthiram, A. Characterization of $GdBa_{1-x}Sr_xCo_2O_{5+\delta}$ ($0 \leq x \leq 1.0$) double perovskites as cathodes for solid oxide fuel cells. *J. Electrochem. Soc.* **2008**, *155*, B1023–B1028. [CrossRef]
87. Kim, J.-H.; Cassidy, M.; Irvine, J.T.S.; Bae, J. Advanced electrochemical properties of $LnBa_{0.5}Sr_{0.5}Co_2O_{5+\delta}$ (Ln = Pr, Sm, and Gd) as cathode materials for IT-SOFC. *J. Electrochem. Soc.* **2009**, *156*, B682–B689. [CrossRef]

88. Subardi, A.; Cheng, M.-H.; Fu, Y.-P. Chemical bulk diffusion and electrochemical properties of $SmBa_{0.6}Sr_{0.4}Co_2O_{5+\delta}$ cathode for intermediate solid oxide fuel cells. *Int. J. Hydrogen Energy* **2014**, *39*, 20783–20790. [CrossRef]
89. Jun, A.; Kim, J.; Shin, J.; Kim, G. Optimization of Sr content in layered $SmBa_{1-x}Sr_xCo_2O_{5+\delta}$ perovskite cathodes for intermediate-temperature solid oxide fuel cells. *Int. J. Hydrogen Energy* **2012**, *37*, 18381–18388. [CrossRef]
90. Lü, S.Q.; Meng, X.W.; Ji, Y.; Fu, C.W.; Sun, C.C.; Zhao, H.Y. Electrochemical performances of $NdBa_{0.5}Sr_{0.5}Co_2O_{5+x}$ as potential cathode material for intermediate-temperature solid oxide fuel cells. *J. Power Sources* **2010**, *195*, 8094–8096. [CrossRef]
91. Yoo, S.; Choi, S.; Kim, J.; Shin, J.; Kim, G. Investigation of layered perovskite type $NdBa_{1-x}Sr_xCo_2O_{5+\delta}$ (x = 0, 0.25, 0.5, 0.75, and 1.0) cathodes for intermediate-temperature solid oxide fuel cells. *Electrochimica Acta* **2013**, *100*, 44–50. [CrossRef]
92. Ding, H.P.; Xue, X.J. $PrBa_{0.5}Sr_{0.5}Co_2O_{5+\delta}$ layered perovskite cathode for intermediate temperature solid oxide fuel cells. *Electrochimica Acta* **2010**, *55*, 3812–3816. [CrossRef]
93. Pang, S.L.; Jiang, X.N.; Li, X.N.; Xu, H.X.; Jiang, L.; Xu, Q.L.; Shi, Y.C.; Zhang, Q.Y. Structure and properties of layered-perovskite $LaBa_{1-x}Co_2O_{5+\delta}$ (x = 0-0.15) as intermediate-temperature cathode material. *J. Power Sources* **2013**, *240*, 54–59. [CrossRef]
94. Pang, S.L.; Jiang, X.N.; Li, X.N.; Wang, Q.; Su, Z.X. Characterization of Ba-deficient $PrBa_{1-x}Co_2O_{5+\delta}$ as cathode material for intermediate temperature solid oxide fuel cells. *J. Power Sources* **2012**, *204*, 53–59. [CrossRef]
95. Pang, S.L.; Jiang, X.N.; Li, X.N.; Wang, Q.; Su, Z.X.; Zhang, Q.Y. Highly enhanced electrochemical performance of $PrBa_{0.92}Co_2O_{5+\delta}$ cathode by introducing Ba cationic-deficiency. *Int. J. Hydrogen Energy* **2012**, *37*, 3998–4001. [CrossRef]
96. Jiang, L.; Li, F.; Wei, T.; Zeng, R.; Huang, Y.H. Evaluation of $Pr_{1+x}Ba_{1-x}Co_2O_{5+\delta}$ (x = 0 − 0.3) as cathode materials for solid-oxide fuel cells. *Electrochimica Acta* **2014**, *133*, 364–372. [CrossRef]
97. Jiang, X.N.; Shi, Y.C.; Zhou, W.L.; Li, X.N.; Su, Z.X.; Pang, S.L.; Jiang, L. Effects of Pr3+-deficiency on structure and properties of $PrBaCo_2O_{5+\delta}$ cathode material-A comparison with Ba2+-deficiency case. *J. Power Sources* **2014**, *272*, 371–377. [CrossRef]
98. Wang, J.P.; Meng, F.C.; Xia, T.; Shi, Z.; Lian, J.; Xu, C.B.; Zhao, H.; Bassat, J.-M.; Grenier, J.-C. Superior electrochemical performance and oxygen reduction kinetics of layered perovskite. *Int. J. Hydrogen Energy* **2014**, *39*, 18392–18404. [CrossRef]
99. Yoo, S.; Jun, A.; Ju, Y.-W.; Odkhuu, D.; Hyodo, J.; Jeong, H.Y.; Park, N.; Shin, J.; Ishihara, T.; Kim, G. Development of Double-perovskite compounds as cathode materials for low-temperature solid oxide fuel cells. *Angew. Chem. Int. Ed.* **2014**, *53*, 13064–13067. [CrossRef]
100. Zhao, L.; Shen, J.C.; He, B.B.; Chen, F.L.; Xia, C.R. Synthesis, characterization and evaluation of $PrBaCo_{2-x}Fe_xO_{5+\delta}$ as cathodes for intermediate-temperature solid oxide fuel cells. *Int. J. Hydrogen Energy* **2011**, *36*, 3658–3665. [CrossRef]
101. Kim, Y.N.; Kim, J.-H.; Manthiram, A. Effects of Fe substitution on the structure and properties of $LnBaCo_{2-x}Fe_xO_{5+\delta}$ (Ln = Nd and Gd) cathodes. *J. Power Sources* **2010**, *195*, 6411–6419. [CrossRef]
102. Jun, A.; Lim, T.-H.; Shin, J.; Kim, G. Electrochemical properties of B-site Ni doped layered perovskite cathodes for IT-SOFCs. *Int. J. Hydrogen Energy* **2014**, *39*, 20791–20798. [CrossRef]
103. Hu, Y.; Bogicevic, C.; Bouffanais, Y.; Giot, M.; Hernandez, O.; Dezanneau, G. Synthesis, physical-chemical characterization and electrochemical performance of $GdBaCo_{2-x}Ni_xO_5$ (x = 0-0.8) as cathode materials for IT-SOFC application. *J. Power Sources* **2013**, *242*, 50–56. [CrossRef]
104. Wei, B.; Lü, Z.; Jia, D.C.; Huang, X.Q.; Zhang, Y.H.; Su, W.H. Thermal expansion and electrochemical properties of Ni-doped $GdBaCo_2O_{5+\delta}$ double-perovskite type oxides. *Int. J. Hydrogen Energy* **2010**, *35*, 3775–3782. [CrossRef]
105. Kim, J.-H.; Manthiram, A. Layered $LnBaCo_{2-x}Ni_xO_{5+\delta}$ ($0 \leq x \leq 1.0$) perovskite cathodes for intermediate temperature solid oxide fuel cells. *J. Electrochem. Soc.* **2011**, *158*, B276–B282. [CrossRef]
106. Lü, S.Q.; Long, G.H.; Ji, Y.; Meng, X.W.; Zhao, H.Y.; Sun, C.C. $SmBaCoCuO_{5+x}$ as cathode material based on GDC electrolyte for intermediate-temperature solid oxide fuel cells. *J. Alloy Compd.* **2011**, *509*, 2824–2828. [CrossRef]
107. Jo, S.H.; Muralidharan, P.; Kim, D.K. Enhancement of electrochemical performance and thermal compatibility of $GdBaCo_{2/3}Fe_{2/3}Cu_{2/3}O_{5+\delta}$ cathode on $Ce_{1.9}Gd_{0.1}O_{1.95}$ electrolyte for IT-SOFCs. *Electrochem. Commun.* **2009**, *11*, 2085–2088. [CrossRef]
108. Choi, S.; Yoo, S.; Kim, J.; Park, S.; Jun, A.; Sengodan, S.; Kim, J.; Shin, J.; Jeong, H.Y.; Choi, Y.; et al. Highly efficient and robust cathode materials for low-temperature solid oxide fuel cells: $PrBa_{0.5}Sr_{0.5}Co_{2-x}Fe_xO_{5+\delta}$. *Sci. Rep.* **2013**, *3*, 2426. [CrossRef] [PubMed]
109. Kim, J.; Jun, A.; Shin, J.; Kim, G. Effect of Fe Doping on Layered $GdBa_{0.5}Sr_{0.5}Co_2O_{5+\delta}$ Perovskite cathodes for intermediate temperature solid oxide fuel cells. *J. Am. Ceram. Soc.* **2014**, *97*, 651–656. [CrossRef]
110. Kim, J.; Choi, S.; Park, S.; Kim, C.; Shin, J.; Kim, G. Effect of Mn on the electrochemical properties of a layered perovskite $NdBa_{0.5}Sr_{0.5}Co_{2-x}Mn_xO_{5+\delta}$ (x = 0, 0.25, and 0.5) for intermediate-temperature solid oxide fuel cells. *Electrochim. Acta* **2013**, *112*, 712–718. [CrossRef]
111. Pramana, S.S.; Cavallaro, A.; Li, C.; Handoko, A.D.; Chan, K.W.; Walker, R.J.; Regoutz, A.; Herrin, J.S.; Yeo, B.S.; Payne, D.J.; et al. Crystal structure and surface characteristics of Sr-doped $GdBaCo_2O_{6-\delta}$ double perovskites: Oxygen evolution reaction and conductivity. *J. Mater. Chem. A* **2018**, *6*, 5335–5345. [CrossRef]
112. Subardi, A.; Chen, C.C.; Cheng, M.H.; Chang, W.K.; Fu, Y.P. Electrical, thermal and electrochemical properties of $SmBa_{1-x}Sr_xCo_2O_{5+\delta}$ cathode materials for intermediate-temperature solid oxide fuel cells. *Electrochim. Acta* **2016**, *204*, 118–127. [CrossRef]
113. Xue, J.; Shen, Y.; He, T. Performance of double-perovskite $YBa_{0.5}Sr_{0.5}Co_2O_{5+\delta}$ as cathode material for intermediate-temperature solid oxide fuel cells. *Int. J. Hydrogen Energy* **2011**, *36*, 6894–6898. [CrossRef]

114. Subardi, A.; Indra, A.; Setiawan, J.; Fu, Y.-P. Structural and Electrochemical Analysis of $SmBa_{0.8}Sr_{0.2}Co_2O_{5+\delta}$ Cathode Oxide for IT-SOFCs. *Int. J. Integr. Eng.* **2023**, *15*, 173–179. [CrossRef]
115. Zan, J.; Wang, S.; Zheng, D.; Li, F.; Chen, W.; Pei, Q.; Jiang, L. Characterization and functional application of $PrBa_{0.5}Sr_{0.5}Co_{1.5}Fe_{0.5}O_{5+\delta}$ cathode material for IT-SOFC. Mater. *Res. Bull.* **2021**, *137*, 111173. [CrossRef]
116. Costilla-Aguilar, S.U.; Escudero, M.J.; Cienfuegos-Pelaes, R.F.; Aguilar-Martinez, J.A. Double perovskite $La_{1.8}Sr_{0.2}CoFeO_{5+\delta}$ as a cathode material for intermediate temperature solid oxide fuel cells. *J. Alloys Compd.* **2021**, *862*, 158025. [CrossRef]
117. Liu, Y.; Cao, Y.; Sun, S.; Lu, C.; Wang, B.; Liu, G.; Gao, S.; Niu, B. Novel CO_2-tolerant Co-based double perovskite cathode for intermediate temperature solid oxide fuel cells. *J. Eur. Ceram. Soc.* **2023**, *43*, 1028–1038. [CrossRef]
118. Li, M.; Chen, K.; Hua, B.; Luo, J.-l.; Rickard, W.D.A.; Li, J.; Irvine, J.T.S.; Jiang, S.P. Smart utilization of cobaltite-based double perovskite cathodes on barrier-layer-free zirconia electrolyte of solid oxide fuel cells. *J. Mater. Chem. A* **2016**, *4*, 19019–19025. [CrossRef]
119. Liu, Z.; Cheng, L.Z.; Han, M.-F. A-site deficient $Ba_{1-x}Co_{0.7}Fe_{0.2}Ni_{0.1}O_{3-\delta}$ cathode for intermediate temperature SOFC. *J. Power Sources* **2011**, *196*, 868–871. [CrossRef]
120. Chen, T.; Pang, S.; Shen, X.; Jiang, X.; Wang, W. Evaluation of Ba-deficient $PrBa_{1-x}Fe_2O_{5+\delta}$ oxides as cathode materials for intermediate-temperature solid oxide fuel cells. *RSC Adv.* **2016**, *6*, 13829–13836. [CrossRef]
121. Yao, C.; Yang, J.; Zhang, H.; Chen, S.; Lang, X.; Meng, J.; Cai, K. Evaluation of A-site Ba-deficient $PrBa_{0.5-x}Sr_{0.5}Co_2O_{5+\delta}$ (x = 0, 0.04 and 0.08) as cathode materials for solid oxide fuel cells. *J. Alloys Compd.* **2021**, *883*, 160759. [CrossRef]
122. Idrees, A.; Jiang, X.; Jiang, L.; Zhang, Q. Properties of composite cathodes composed of Pr^{3+}-deficient perovskite oxide and ionic conductor $Ce_{0.8}Sm_{0.2}O_{1.9}$. *Ceram. Int.* **2020**, *46*, 17532–17539. [CrossRef]
123. Liu, X.; Jin, F.; Sun, N.; Li, J.; Shen, Y.; Wang, F.; Li, J. Nd^{3+}-deficiency double perovskite $Nd_{1-x}BaCo_2O_{5+\delta}$ and performance optimization as cathode materials for intermediate-temperature solid oxide fuel cells. *Ceram. Int.* **2021**, *47*, 33886–33896. [CrossRef]
124. Yi, K.; Sun, L.; Li, Q.; Xia, T.; Huo, L.; Zhao, H.; Li, J.; Lü, Z.; Bassat, J.-M.; Rougier, A.; et al. Effect of Nd-deficiency on electrochemical properties of $NdBaCo_2O_{6-\delta}$ cathode for intermediate-temperature solid oxide fuel cells. *Int. J. Hydrogen Energy* **2016**, *41*, 10228–10238. [CrossRef]
125. Lü, S.; Zhu, Y.; Fu, X.; Huang, R.; Guo, Y.; Zhang, W.; Li, H.; Hou, L.; Meng, X. A-site deficient Fe-based double perovskite oxides $Pr_xBaFe_2O_{5+\delta}$ as cathodes for solid oxide fuel cells. *J. Alloys Compd.* **2022**, *911*, 165002. [CrossRef]
126. Nie, Z.; Wang, J.; Xia, T.; Wang, G. A-site Ca-doped layered double perovskite $Pr_{1-x}Ca_xBa_{0.94}Co_2O_{5+\delta}$ as high-performance and stable cathode for intermediate-temperature solid oxide fuel cells. *J. Alloys Compd.* **2022**, *905*, 164191. [CrossRef]
127. Yao, C.; Yang, J.; Zhang, H.; Lang, X.; Cai, K. Ca-doped $PrBa_{1-x}Ca_xCoCuO_{5+\delta}$ (x = 0–0.2) as cathode materials for solid oxide fuel cells. *Ceram. Int.* **2022**, *48*, 7652–7662. [CrossRef]
128. Asensio, A.M.; Clematis, D.; Cademartori, D.; Carpanese, M.P.; Viviani, M.; Carbone, C.; Barbucci, A. Calcium doping in double perovskite $SmBa_{1-x}Ca_xCo_2O_{5+\delta}$ to enhance the electrochemical activity of solid oxide cell reversible oxygen electrode. *J. Alloys Compd.* **2023**, *933*, 167731. [CrossRef]
129. Liu, X.; Jin, F.; Liu, X.; Sun, N.; Li, J.; Shen, Y.; Wang, F.; Yang, L.; Chu, X.; Xu, M.; et al. Effect of calcium doping on $Sm_{1-x}Ca_xBaCo_2O_{5+\delta}$ cathode materials for intermediate-temperature solid oxide fuel cells. *Electrochim. Acta* **2021**, *390*, 138830. [CrossRef]
130. Jin, F.; Liu, X.; Chu, X.; Shen, Y.; Li, J. Effect of nonequivalent substitution of $Pr^{3+/4+}$ with Ca^{2+} in $PrBaCoFeO_{5+\delta}$ as cathodes for IT-SOFC. *J. Mater. Sci.* **2021**, *56*, 1147–1161. [CrossRef]
131. Du, Z.; Yan, C.; Zhao, H.; Zhang, Y.; Yang, C.; Yi, S.; Lu, Y.; Świerczek, K. Effective Ca-doping in $Y_{1-x}Ca_xBaCo_2O_{5+\delta}$ cathode materials for intermediate temperature solid oxide fuel cells. *J. Mater. Chem. A* **2017**, *5*, 25641–25651. [CrossRef]
132. Pang, S.; Su, Y.; Yang, G.; Shen, X.; Zhu, M.; Wu, X.; Li, S.; Yang, X.; Xi, X. Enhanced electrochemical performance of Ca-doped $NdBa_{1-x}Ca_xCoCuO_{5+\delta}$ as cathode material for intermediate-temperature solid oxide fuel cells. *Ceram. Int.* **2018**, *44*, 21902–21907. [CrossRef]
133. Xia, W.; Liu, X.; Jin, F.; Jia, X.; Shen, Y.; Li, J. Evaluation of calcium codoping in double perovskite $PrBaCo_2O_{5+\delta}$ as cathode material for IT-SOFCs. *Electrochim. Acta* **2020**, *364*, 137274. [CrossRef]
134. Li, J.; Sun, N.; Liu, X.; Shen, Y.; Wang, F.; Li, J.; Shi, K.; Jin, F. Investigation on $Nd_{1-x}Ca_xBaCo_2O_{5+\delta}$ double perovskite as new oxygen electrode materials for reversible solid oxide cells. *J. Alloys Compd.* **2022**, *913*, 165245. [CrossRef]
135. Wang, L.; Xie, P.; Bian, L.; Liu, X.; Chou, K. Performance of Ca-doped $GdBa_{1-x}Ca_xFe_2O_{5+\delta}$ (x=0, 0.1) as cathode materials for IT-SOFC application. *Catal. Today* **2018**, *318*, 132–136. [CrossRef]
136. Xiang, W.; Wang, J.; Li, S.; Xia, T.; Wang, G. Positive effects of calcium-doping on the cathode performance of layered perovskite $Eu_{1-x}Ca_xBaCo_2O_{5+\delta}$ for intermediate-temperature solid oxide fuel cells. *J. Alloys Compd.* **2019**, *801*, 220–228. [CrossRef]
137. Wang, W.; Pang, S.; Su, Y.; Shen, X.; Wang, Y.; Xu, K.; Xi, X.; Xiang, J. The effect of calcium on the properties of $SmBa_{1-x}Ca_xCoCuO_{5+\delta}$ as a cathode material for intermediate-temperature solid oxide fuel cells. *J. Eur. Ceram. Soc.* **2017**, *37*, 1557–1562. [CrossRef]
138. Zhou, D.; Yuan, C.; Chen, X.; Chen, F.; Xiong, X.; Liu, Y.; Yan, J.; Fujita, T. A-site double-lanthanide-doped $La_{1-x}Pr_xBaCo_2O_{5+\delta}$ cathode materials for intermediate-temperature solid oxide fuel cells. *J. Mater. Sci.* **2022**, *57*, 14398–14412. [CrossRef]

139. Bangwal, A.S.; Jha, P.K.; Chauhan, M.; Singh, S.; Sinha, A.S.K.; Jha, P.A.; Singh, P. Compositional effect on oxygen reduction reaction in Pr excess double perovskite $Pr_{1-x}Ba_{1-x}Co_2O_{6-\delta}$ cathode materials. *Int. J. Hydrogen Energy* **2020**, *45*, 23378–23390. [CrossRef]
140. Chen, F.; Zhou, D.; Xiong, X.; Pan, J.; Cai, D.; Wei, Z.; Chen, X.; Liu, Y.; Luo, N.; Yan, J.; et al. Doping strategy on improving the overall cathodic performance of double perovskite $LnBaCo_2O_{5+\delta}$ (Ln=Pr, Gd) as potential SOFC cathode materials. *J. Mater*. **2023**, *9*, 825–837. [CrossRef]
141. Zhu, F.; He, F.; Xu, K.; Chen, Y. Enhancing the oxygen reduction reaction activity and durability of a double-perovskite via an A-site tuning. *Sci. China Mater.* **2022**, *65*, 3043–3052. [CrossRef]
142. Wang, S.; Zan, J.; Qiu, W.; Zheng, D.; Li, F.; Chen, W.; Pei, Q.; Jiang, L. Evaluation of perovskite oxides $LnBaCo_2O_{5+\delta}$ (Ln = La, Pr, Nd and Sm) as cathode materials for IT-SOFC. *J. Electroanal. Chem.* **2021**, *886*, 115144. [CrossRef]
143. Yang, Q.; Tian, D.; Liu, R.; Wu, H.; Chen, Y.; Ding, Y.; Lu, X.; Lin, B. Exploiting rare-earth-abundant layered perovskite cathodes of $LnBa_{0.5}Sr_{0.5}Co_{1.5}Fe_{0.5}O_{5+\delta}$ (Ln=La and Nd) for SOFCs. *Int. J. Hydrogen Energy* **2021**, *46*, 5630–5641. [CrossRef]
144. Zhang, Y.; Niu, B.; Hao, X.; Wang, Y.; Liu, J.; Jiang, P.; He, T. Layered oxygen-deficient double perovskite $GdBaFe_2O_{5+\delta}$ as electrode material for symmetrical solid-oxide fuel cells. *Electrochim. Acta* **2021**, *370*, 137807. [CrossRef]
145. Saccoccio, M.; Jiang, C.; Gao, Y.; Chen, D.; Ciucci, F. Nb-substituted $PrBaCo_2O_{5+\delta}$ as a cathode for solid oxide fuel cells: A systematic study of structural, electrical, and electrochemical properties. *Int. J. Hydrogen Energy* **2017**, *42*, 19204–19215. [CrossRef]
146. Akande, S.O.; Chroneos, A.; Schwingenschlögl, U. O vacancy formation in (Pr/Gd)$BaCo_2O_{5.5}$ and the role of antisite defects. *Phys. Chem. Chem. Phys.* **2017**, *19*, 11455–11459. [CrossRef] [PubMed]
147. Anjum, U.; Vashishtha, S.; Agarwal, M.; Tiwari, P.; Sinha, N.; Agrawal, A.; Basu, S.; Haider, M.A. Oxygen anion diffusion in double perovskite $GdBaCo_2O_{5+\delta}$ and $LnBa_{0.5}Sr_{0.5}Co_{2-x}Fe_xO_{5+\delta}$ (Ln = Gd, Pr, Nd) electrodes. *Int. J. Hydrogen Energy* **2016**, *41*, 7631–7640. [CrossRef]
148. Ananyev, M.V.; Eremin, V.A.; Tsvetkov, D.S.; Porotnikova, N.M.; Farlenkov, A.S.; Zuev, A.Y.; Fetisov, A.V.; Kurumchin, E.K. Oxygen isotope exchange and diffusion in $LnBaCo_2O_{6-\delta}$ (Ln = Pr, Sm, Gd) with double perovskite structure. *Solid State Ionics* **2017**, *304*, 96–106. [CrossRef]
149. Zhou, Q.; Wang, F.; Shen, Y.; He, T. Performances of $LnBaCo_2O_{5+x}$–$Ce_{0.8}Sm_{0.2}O_{1.9}$ composite cathodes for intermediate-temperature solid oxide fuel cells. *J. Power Sources* **2010**, *195*, 2174–2181. [CrossRef]
150. Malyshkin, D.; Novikov, A.; Tsvetkov, D.; Zuev, A. Preparation, oxygen nonstoichiometry and defect structure of double perovskite $LaBaCo_2O_{6-\delta}$. *Mater. Lett.* **2018**, *229*, 324–326. [CrossRef]
151. Liu, S.; Zhang, W.; Li, Y.; Yu, B. $REBaCo_2O_{5+\delta}$ (RE = Pr, Nd, and Gd) as promising oxygen electrodes for intermediate-temperature solid oxide electrolysis cells. *RSC Adv.* **2017**, *7*, 16332–16340. [CrossRef]
152. Politov, B.V.; Suntsov, A.Y.; Leonidov, I.A.; Patrakeev, M.V.; Kozhevnikov, V.L. Thermodynamic analysis of defect equilibration in double perovskites based on $PrBaCo_2O_{6-\delta}$ cobaltite. *J. Solid State Chem.* **2017**, *249*, 108–113. [CrossRef]
153. Jin, F.; Liu, J.; Shen, Y.; He, T. Improved electrochemical performance and thermal expansion compatibility of $LnBaCoFeO_{5+\delta}$-$Sm_{0.2}Ce_{0.8}O_{1.9}$ (Ln=Pr and Nd) composite cathodes for IT-SOFCs. *J. Alloys Compd.* **2016**, *685*, 483–491. [CrossRef]
154. Zając, W.; Świerczek, K.; Molenda, J. Thermochemical compatibility between selected (La,Sr)(Co,Fe,Ni)O_3 cathodes and rare earth doped ceria electrolytes. *J. Power Sources* **2007**, *173*, 675–680. [CrossRef]
155. Zhu, J.H.; Geng, S.J.; Ballard, D.A. Evaluation of several low thermal expansion Fe–Co–Ni alloys as interconnect for reduced-temperature solid oxide fuel cell. *Int. J. Hydrogen Energy* **2007**, *32*, 3682–3688. [CrossRef]
156. Señarís-Rodríguez, M.A.; Goodenough, J.B. Magnetic and Transport Properties of the System $La_{1-x}Sr_xCoO_{3-\delta}$ ($0 < x \leq 0.50$). *J. Solid State Chem.* **1995**, *118*, 323–336. [CrossRef]
157. Huang, K.; Lee, H.Y.; Goodenough, J.B. Sr- and Ni- Doped $LaCoO_3$ and $LaFeO_3$ perovskites: New cathode materials for solid-oxide fuel cells. *J. Electrochem. Chem.* **1998**, *145*, 3220–3227. [CrossRef]
158. Tsvetkov, D.S.; Ivanov, I.L.; Zuev, A.Y. Crystal structure and oxygen content of the double perovskites $GdBaCo_{2-x}Fe_xO_{6-\delta}$. *J. Solid State Chem.* **2013**, *199*, 154–159. [CrossRef]
159. Xue, J.; Shen, Y.; He, T. Double-perovskites $YBaCo_{2-x}Fe_xO_{5+\delta}$ cathodes for intermediate-temperature solid oxide fuel cells. *J. Power Sources* **2011**, *196*, 3729–3735. [CrossRef]
160. Zou, J.; Park, J.; Kwak, B.; Yoon, H.; Chung, J. Effect of Fe doping on $PrBaCo_2O_{5+\delta}$ as cathode for intermediate-temperature solid oxide fuel cells. *Solid State Ionics* **2012**, *206*, 112–119. [CrossRef]
161. Joo, S.; Kim, J.; Shin, J.; Lim, T.-H.; Kim, G. Investigation of a layered perovskite for IT-SOFC cathodes: B-site Fe-doped $YBa_{0.5}Sr_{0.5}Co_{2-x}Fe_xO_{5+\delta}$. *J. Electrochem. Soc.* **2016**, *163*, F1489–F1495. [CrossRef]
162. Son, S.J.; Kim, D.; Park, H.J.; Joo, J.H. Investigation of oxygen ion transport and surface exchange properties of $PrBaFe_2O_{5+\delta}$. *J. Eur. Ceram. Soc.* **2021**, *41*, 2691–2698. [CrossRef]
163. Zhang, H.-X.; Yang, J.-X.; Wang, P.-F.; Yao, C.-G.; Yu, X.-D.; Shi, F.-N. Novel cobalt-free perovskite $PrBaFe_{1.9}Mo_{0.1}O_{5+\delta}$ as a cathode material for solid oxide fuel cells. *Solid State Ionics* **2023**, *391*, 116144. [CrossRef]
164. Politov, B.V.; Suntsov, A.Y.; Leonidov, I.A.; Patrakeev, M.V.; Kozhevnikov, V.L. High-temperature defect thermodynamics of nickel substituted double-perovskite cobaltite $PrBaCo_{2-x}Ni_xO_{6-\delta}$ (x = 0.2). *J. Alloys Compd.* **2017**, *727*, 778–784. [CrossRef]
165. Xia, L.-N.; You, J.; He, Z.-P.; Huang, X.-W.; Yu, Y. Performances of nickel-doped $SmBaCo_2O_{5+\delta}$-$Sm_{0.2}Ce_{0.8}O_{1.9}$ composite cathodes for IT-SOFC. *Int. J. Hydrogen Energy* **2016**, *41*, 1176–1186. [CrossRef]

166. Xia, L.-N.; He, Z.-P.; Huang, X.W.; Yu, Y. Synthesis and properties of $SmBaCo_{2-x}Ni_xO_{5+\delta}$ perovskite oxide for IT-SOFC cathodes. *Ceram. Int.* **2016**, *42*, 1272–1280. [CrossRef]
167. Garcia-Garcia, F.J.; Sayagués, M.J.; Gotor, F.J. A Novel, Simple and highly efficient route to obtain $PrBaMn_2O_{5+\delta}$ double perovskite: Mechanochemical synthesis. *Nanomaterials* **2021**, *11*, 380. [CrossRef]
168. Huang, X.; Feng, J.; Abdellatif, H.R.S.; Zou, J.; Zhang, G.; Ni, C. Electrochemical evaluation of double perovskite $PrBaCo_{2-x}Mn_xO_{5+\delta}$ (x = 0, 0.5, 1) as promising cathodes for IT-SOFCs. *Int. J. Hydrogen Energy* **2018**, *43*, 8962–8971. [CrossRef]
169. Ren, R.; Wang, Z.; Meng, X.; Xu, C.; Qiao, J.; Sun, W.; Sun, K. Boosting the electrochemical performance of Fe-based layered double perovskite cathodes by Zn^{2+} doping for solid oxide fuel cells. *ACS Appl. Mater. Interfaces* **2020**, *12*, 23959–23967. [CrossRef]
170. Sun, C.; Kong, Y.; Niu, Y.; Yin, X.; Zhang, N. Probing Zr substituting effects on the oxygen reduction reaction of Fe-based double perovskite cathodes for solid oxide fuel cells. *ACS Appl. Energy Mater.* **2022**, *5*, 4486–4495. [CrossRef]
171. Sun, C.; Kong, Y.; Shao, L.; Zhang, Q.; Wu, X.; Zhang, N.; Sun, K. Significant zirconium substitution effect on the oxygen reduction activity of the cathode material $NdBaCo_2O_{5+\delta}$ for solid oxide fuel cells. *ACS Sust. Chem. Eng.* **2019**, *7*, 11603–11611. [CrossRef]
172. Zhang, B.; Wan, Y.; Hua, Z.; Tang, K.; Xia, C. Tungsten-doped $PrBaFe_2O_{5+\delta}$ double perovskite as a high-performance electrode material for symmetrical solid oxide fuel cells. *ACS Appl. Energy Mater.* **2021**, *4*, 8401–8409. [CrossRef]
173. Jeong, D.; Kim, J.; Kwon, O.; Lim, C.; Sengodan, S.; Shin, J.; Kim, G. Scandium doping effect on a layered perovskite cathode for low-temperature solid oxide fuel cells (LT-SOFCs). *Appl. Sci.* **2018**, *8*, 2217. [CrossRef]
174. Xu, J.; Cai, H.; Hao, G.; Zhang, L.; Song, Z.; Long, W.; Zhang, L.; Wang, L. Characterization of high-valence Mo-doped $PrBaCo_2O_{5+\delta}$ cathodes for IT-SOFCs. *J. Alloys Compd.* **2020**, *842*, 155600. [CrossRef]
175. Zhang, B.; Zhang, S.; Han, H.; Tang, K.; Xia, C. Cobalt-free double perovskite oxide as a promising cathode for solid oxide fuel cells. *ACS Appl. Mater. Interfaces* **2023**, *15*, 8253–8262. [CrossRef]
176. Bao, X.; Su, X.; Wang, S.; Pan, B.; Wang, L.; Zhang, L.; Song, Z.; Long, W.; Li, C. Effects of Bi-doping on structure and properties of $YBaCo_2O_{5+\delta}$ layered perovskite cathode for intermediate-temperature solid oxide fuel cells. *J. Alloys Compd.* **2023**, *965*, 171391. [CrossRef]
177. Pelosato, R.; Cordaro, G.; Stucchi, D.; Cristiani, C.; Dotelli, G. Cobalt based layered perovskites as cathode material for intermediate temperature solid oxide fuel cells: A brief review. *J. Power Sources* **2015**, *298*, 46–67. [CrossRef]
178. Zheng, Y.; Zhang, Y.; Yu, F.; Pan, Z.; Yang, H.; Guo, L. Ca and Fe co-doped $SmBaCo_2O_{5+\delta}$ layered perovskite as an efficient cathode for intermediate-temperature solid oxide fuel cells. *J. Alloys Compd.* **2017**, *696*, 964–970. [CrossRef]
179. Tian, Y.; Liu, Y.; Wang, W.; Jia, L.; Pu, J.; Chi, B.; Li, J. High performance and stability of double perovskite-type oxide $NdBa_{0.5}Ca_{0.5}Co_{1.5}Fe_{0.5}O_{5+\delta}$ as an oxygen electrode for reversible solid oxide electrochemical cell. *J. Energy Chem.* **2020**, *43*, 108–115. [CrossRef]
180. Liu, B.; Yang, J.; Yan, D.; Jia, L.; Chi, B.; Pu, J.; Li, J. Novel $PrBa_{0.9}Ca_{0.1}Co_{2-x}Zn_xO_{5+\delta}$ double-perovskite as an active cathode material for high-performance proton-conducting solid oxide fuel cells. *Int. J. Hydrogen Energy* **2020**, *45*, 31009–31016. [CrossRef]
181. Dong, F.F.; Ni, M.; Chen, Y.B.; Chen, D.J.; Tadé, M.O.; Shao, Z.P. Structural and oxygen-transport studies of double perovskites $PrBa_{1-x}Co_2O_{5+\delta}$ (x = 0.00, 0.05, and 0.10) toward their application as superior oxygen reduction electrodes. *J. Mater. Chem. A* **2014**, *2*, 20520–20529. [CrossRef]
182. Ding, D.; Li, X.X.; Lai, S.Y.; Gerdes, K.; Liu, M.L. Enhancing SOFC cathode performance by surface modification through infiltration. *Energy Environ. Sci.* **2014**, *7*, 552–575. [CrossRef]
183. Choi, Y.; Choi, S.; Jeong, H.Y.; Liu, M.L.; Kim, B.-S.; Kim, G. Highly efficient layer-by-layer-assisted infiltration for high-performance and cost-effective fabrication of nanoelectrodes. *ACS Appl. Mater. Interfaces* **2014**, *6*, 17352–17357. [CrossRef]
184. Han, D.; Wu, H.; Li, J.L.; Wang, S.R.; Zhan, Z.L. Nanostructuring of $SmBa_{0.5}Sr_{0.5}Co_2O_{5+\delta}$ cathodes for reduced-temperature solid oxide fuel cells. *J. Power Sources* **2014**, *246*, 409–416. [CrossRef]
185. Ding, H.P.; Xue, X.J. An Interfacial nanospike-structured cathode for low temperature solid oxide fuel cells. *Adv. Mater. Interfaces* **2014**, *1*, 1400008. [CrossRef]
186. Gao, Y.; Chen, D.J.; Chen, C.; Shao, Z.P.; Ciucci, F. Oriented $PrBaCo_2O_{5+\delta}$ thin films for solid oxide fuel cells. *J. Power Sources* **2015**, *278*, 623–629. [CrossRef]
187. Liu, J.; Collins, G.; Liu, M.; Chen, C.L. Superfast oxygen exchange kinetics on highly epitaxial $LaBaCo_2O_{5+\delta}$ thin films for intermediate temperature solid oxide fuel cells. *APL Mater.* **2013**, *1*, 031101. [CrossRef]
188. Liu, J.; Collins, G.; Liu, M.; Chen, C.L.; He, J.; Jiang, J.C.; Meletis, E.I. Ultrafast oxygen exchange kinetics on highly epitaxial $PrBaCo_2O_{5+\delta}$ thin films. *Appl. Phys. Lett.* **2012**, *100*, 193903. [CrossRef]
189. Pang, S.; Long, C.; Tang, X.; Fang, T.; Ke, L.; Yang, G.; Song, Y.; Chen, C. Highly active and robust biomimetic ceramic catalyst for oxygen reduction reaction: Inspired by plant leaves. *Ceram. Int.* **2023**, *49*, 20273–20280. [CrossRef]
190. Kim, S.; Jun, A.; Kwon, O.; Kim, J.; Yoo, S.; Jeong, H.Y.; Shin, J.; Kim, G. Nanostructured double perovskite cathode with low sintering temperature for intermediate temperature solid oxide fuel cells. *ChemSusChem* **2015**, *8*, 3153–3158. [CrossRef]
191. Tsvetkov, D.S.; Ivanov, I.L.; Malyshkin, D.A.; Zuev, A.Y. Oxygen content, cobalt oxide exsolution and defect structure of the double perovskite $PrBaCo_2O_{6-\delta}$. *J. Mater. Chem. A* **2016**, *4*, 1962–1969. [CrossRef]
192. Pang, S.; Song, Y.; Cui, M.; Tang, X.; Long, C.; Ke, L.; Yang, G.; Fang, T.; Guan, Y.; Chen, C. Rapid and durable oxygen reduction reaction enabled by a perovskite oxide with self-cleaning surface. *J. Energy Chem.* **2023**, *83*, 333–340. [CrossRef]
193. Fu, M.; Lin, X.; Tan, L.; Zhang, P.; Xie, H.; Tao, Z. Self-assembled Fe-doped $PrBaCo_2O_{5+\delta}$ composite cathodes with disorder transition region for intermediate-temperature solid oxide fuel cells. *Int. J. Hydrogen Energy* **2023**, *48*, 15229–15237. [CrossRef]

194. Jiang, X.N.; Xu, H.X.; Wang, Q.; Jiang, L.; Li, X.N.; Xu, Q.L.; Shi, Y.C.; Zhang, Q.Y. Fabrication of $GdBaCo_2O_{5+\delta}$ cathode using electrospun composite nanofibers and its improved electrochemical performance. *J. Alloys Compd.* **2013**, *557*, 184–189. [CrossRef]
195. Hedayat, N.; Du, Y.; Ilkhani, H. Review on fabrication techniques for porous electrodes of solid oxide fuel cells by sacrificial template methods. *Renew. Sust. Energ. Rev.* **2017**, *77*, 1221–1239. [CrossRef]
196. Chen, Y.; Bu, Y.; Zhao, B.; Zhang, Y.; Ding, D.; Hu, R.; Wei, T.; Rainwater, B.; Ding, Y.; Chen, F.; et al. A durable, high-performance hollow-nanofiber cathode for intermediate-temperature fuel cells. *Nano Energy* **2016**, *26*, 90–99. [CrossRef]
197. Fan, L.; Zhu, B.; Su, P.-C.; He, C. Nanomaterials and technologies for low temperature solid oxide fuel cells: Recent advances, challenges and opportunities. *Nano Energy* **2018**, *45*, 148–176. [CrossRef]
198. Zhang, Y.; Knibbe, R.; Sunarso, J.; Zhong, Y.; Zhou, W.; Shao, Z.; Zhu, Z. Recent progress on advanced materials for solid-oxide fuel cells operating below 500 °C. *Adv. Mater.* **2017**, *29*, 1700132. [CrossRef]
199. Xu, X.; Wang, W.; Zhou, W.; Shao, Z. Recent advances in novel nanostructuring methods of perovskite electrocatalysts for energy-related applications. *Small Methods* **2018**, *2*, 1800071. [CrossRef]
200. Huang, X.; Zhao, G.; Wang, G.; Irvine, J.T.S. Synthesis and applications of nanoporous perovskite metal oxides. *Chem. Sci.* **2018**, *9*, 3623–3637. [CrossRef]
201. Zhen, D.; Zhao, B.; Shin, H.-C.; Bu, Y.; Ding, Y.; He, G.; Liu, M. Electrospun porous perovskite $La_{0.6}Sr_{0.4}Co_{1-x}Fe_xO_{3-\delta}$ nanofibers for efficient oxygen evolution reaction. *Adv. Mater. Interfaces* **2017**, *4*, 1700146. [CrossRef]
202. Wang, Y.; Arandiyan, H.; Tahini, H.A.; Scott, J.; Tan, X.; Dai, H.; Gale, J.D.; Rohl, A.L.; Smith, S.C.; Amal, R. The controlled disassembly of mesostructured perovskites as an avenue to fabricating high performance nanohybrid catalysts. *Nat. Commun.* **2017**, *8*, 15553. [CrossRef] [PubMed]
203. Zou, Q.; Liu, M.; Wang, G.Q.; Lu, H.L.; Yang, T.Z.; Guo, H.M.; Ma, C.R.; Xu, X.; Zhang, M.H.; Jiang, J.C.; et al. Step terrace tuned anisotropic transport properties of highly epitaxial $LaBaCo_2O_{5.5+\delta}$ thin films on vicinal $SrTiO_3$ substrates. *ACS Appl. Mater. Interfaces* **2014**, *6*, 6704–6708. [CrossRef] [PubMed]
204. Liu, J.; Liu, M.; Collins, G.; Chen, C.L.; Jiang, X.N.; Gong, W.Q.; Jacobson, A.J.; He, J.; Jiang, J.C.; Meletis, E.I. Epitaxial nature and transport properties in $(LaBa)Co_2O_{5+\delta}$ thin films. *Chem. Mater.* **2010**, *22*, 799–802. [CrossRef]
205. Druce, J.; Téllez, H.; Burriel, M.; Sharp, M.D.; Fawcett, L.J.; Cook, S.N.; Mcphail, D.S.; Ishihara, T.; Brongersma, H.H.; Kilner, J.A. Surface termination and subsurface restructuring of perovskite-based solid oxide electrode materials. *Energy Environ. Sci.* **2014**, *7*, 3593–3599. [CrossRef]
206. Lee, W.; Yildiz, B. Factors that influence cation segregation at the surfaces of perovskite oxides. *ECS Trans.* **2013**, *57*, 2115–2123. [CrossRef]
207. Lee, W.; Han, J.W.; Chen, Y.; Cai, Z.H.; Yildiz, B. Cation size mismatch and charge interactions drive dopant segregation at the surfaces of manganite perovskites. *J. Am. Chem. Soc.* **2013**, *135*, 7909–7925. [CrossRef]
208. Mebane, D.S. A variational approach to surface cation segregation in mixed conducting perovskites. *Comput. Mater. Sci.* **2014**, *103*, 231–236. [CrossRef]
209. Pang, S.; Xu, J.; Su, Y.; Yang, G.; Zhu, M.; Cui, M.; Shen, X.; Chen, C. The role of A-site cation size mismatch in tune the catalytic activity and durability of double perovskite oxides. *Appl. Catal. B Environ.* **2020**, *270*, 118868. [CrossRef]
210. Anjum, U.; Agarwal, M.; Khan, T.S.; Haider, M.A. Mechanistic elucidation of surface cation segregation in double perovskite $PrBaCo_2O_{5+\delta}$ material using MD and DFT simulations for solid oxide fuel cells. *Ionics* **2020**, *26*, 1307–1314. [CrossRef]
211. Zhu, L.; Wei, B.; Lü, Z.; Feng, J.; Xu, L.; Gao, H.; Zhang, Y.; Huang, X. Performance degradation of double-perovskite $PrBaCo_2O_{5+\delta}$ oxygen electrode in CO_2 containing atmospheres. *Appl. Surf. Sci.* **2017**, *416*, 649–655. [CrossRef]
212. Wei, B.; Chen, K.; Wang, C.C.; Lü, Z.; Jiang, S.P. Performance degradation of $SmBaCo_2O_{5+\delta}$ cathode induced by chromium deposition for solid oxide fuel cells. *Electrochim. Acta* **2015**, *174*, 327–331. [CrossRef]
213. Kim, J.H.; Yoo, S.; Murphy, R.; Chen, Y.; Ding, Y.; Pei, K.; Zhao, B.; Kim, G.; Choi, Y.M.; Liu, M. Promotion of oxygen reduction reaction on a double perovskite electrode by a water-induced surface modification. *Energy Environ. Sci.* **2021**, *14*, 1506–1516. [CrossRef]
214. Wei, B.; Schroeder, M.; Martin, M. Surface cation segregation and chromium deposition on the double perovskite oxide $PrBaCo_2O_{5+\delta}$. *ACS Appl. Mater. Interfaces* **2018**, *10*, 8621–8629. [CrossRef] [PubMed]
215. Druce, J.; Téllez, H.; Hyodo, J. Surface segregation and poisoning in materials for low-temperature SOFCs. *MRS Bull.* **2014**, *39*, 810–815. [CrossRef]
216. Lu, F.; Xia, T.; Li, Q.; Wang, J.; Huo, L.; Zhao, H. Heterostructured simple perovskite nanorod-decorated double perovskite cathode for solid oxide fuel cells: Highly catalytic activity, stability and CO_2-durability for oxygen reduction reaction. *Appl. Catal. B Environ.* **2019**, *249*, 19–31. [CrossRef]
217. Ke, L.; Pang, S.; Long, C.; Fang, T.; Yang, G.; Song, Y.; He, X.; Ma, S.; Qian, Y.; Shen, X.; et al. Quenching-induced surface reconstruction of perovskite oxide for rapid and durable oxygen catalysis. *Chem. Eng. J.* **2023**, *463*, 142509. [CrossRef]
218. Yang, G.; Xu, J.; Pang, S.; Cui, M.; Shen, X. Tuning interfacial chemistry and electrochemical properties of solid oxide cells via cation interdiffusion. *Ceram. Int.* **2020**, *46*, 12044–12049. [CrossRef]